

Understanding the Mechanism and Importance of Brown Carbon Bleaching Across the Visible Spectrum in Biomass Burning Plumes from the WE-CAN Campaign

Yingjie Shen¹, Rudra P. Pokhrel^{1, a}, Amy P. Sullivan², Ezra J. T. Levin^{2, b}, Lauren A. Garofalo³, Delphine K. Farmer³, Wade Permar⁴, Lu Hu⁴, Darin W. Toohey⁵, Teresa Campos⁶, Emily V. Fischer², Shane M. Murphy¹

¹Department of Atmospheric Science, University of Wyoming, Laramie, WY 82071, USA.

²Department of Atmospheric Science, Colorado State University, Fort Collins, CO 80523, USA

³Department of Chemistry, Colorado State University, Fort Collins, CO 80523, USA

⁴Department of Chemistry and Biochemistry, University of Montana, Missoula, MT 59812, USA.

⁵Department of Atmospheric and Oceanic Sciences, University of Colorado Boulder, Boulder, CO 80309, USA

⁶National Center for Atmospheric Research, Atmospheric Chemistry Division, Boulder, CO 80301, USA

^anow at Air Pollution Control Division, Colorado Department of Public Health and Environment, Denver, CO 80246, USA

^bnow at METEC Research Group, Colorado State University Energy Institute, Fort Collins, CO 80524, USA

Corresponding author: Shane M. Murphy (shane.murphy@uwyo.edu)

Abstract. Aerosol absorption of visible light has an important impact on global radiative forcing. Wildfires are one of the major sources of light-absorbing aerosol, but there remains significant uncertainty about the magnitude, wavelength dependence, and bleaching of absorption from biomass burning aerosol. We collected and analyzed data from 21 Western United States wildfire smoke plumes during the 2018 WE-CAN airborne measurement campaign to determine the contribution of black carbon (BC), brown carbon (BrC), and lensing to the aerosol mass absorption cross-section (MAC). Comparison to commonly used parameterizations and modeling studies suggest model overestimation of absorption is likely due to incorrect BrC refractive indices. Modelers (Wang et al. 2018; Carter et al. 2021) invoke a bleaching process that decreases the MAC of organic aerosol (OA) to offset the overestimation of absorption in models. However, no evidence of decreasing MAC is observed in individual WE-CAN fire plumes or in aged plumes from multiple fires. A decrease in OA mass and water-soluble organic carbon (WSOC), both normalized by CO to correct for dilution, is observed with increasing oxygen to carbon (O:C) ratio and decreasing gas-phase toluene:benzene ratio, when data from all fires is combined and in half of individual fire plumes. This results in a strong decrease in total absorption at 405 nm and slight decrease at 660 nm with these chemical markers. These results demonstrate that changes in absorption with chemical markers of plume age are the result of decreasing OA rather than changes in the MAC of the organic material itself. While decreasing MAC or OA mass with aging could both be called bleaching, and can both correct overestimation of absorption in models, it's important to distinguish these two effects because decreasing OA mass will also decrease scattering, which will cause a significantly different net radiative effect. We also find that an average of 54% of non-BC absorption (23% total absorption) at 660 nm is from water-soluble BrC, confirming that BrC absorption is important across the visible spectrum. Quantification of significant BrC at red wavelengths and the observation of bleaching being caused by changes in OA with O:C and

37 toluene:benzene markers of plume age provide important improvements to our understanding of BrC and critical
38 constraints on aerosol absorption in regional and global climate models.

39 **1 Introduction**

40 Atmospheric aerosol impact the climate system by directly scattering and absorbing solar radiation, by
41 indirectly changing cloud properties, and through deposition that changes the surface albedo (McConnell et al., 2007;
42 Sarangi et al., 2020). Biomass burning injects a large amount of primary organic aerosol (POA), secondary organic
43 aerosol (SOA) and black carbon (BC) into the atmosphere every year. BC is somewhat poorly defined, but is generally
44 considered to be insoluble, refractory, and has an absorption exponent near one. Other materials such as elemental
45 carbon (EC), and soot (Wei et al., 2013) are often very similar to BC, but each is operationally defined by how it is
46 measured. Although it only represents a small fraction of aerosol mass, BC has a significant impact on the global
47 energy budget due to its ability to strongly absorb solar radiation at all visible wavelengths. While still important,
48 positive radiative forcing of BC is lower in IPCC AR6 (2022) than in IPCC AR5 (2013). Bond et al. (2013) estimated
49 the direct radiative forcing for BC from 1750 to 2005 at the top of the atmosphere (TOA) to be $+0.71 \text{ W m}^{-2}$, with an
50 uncertainty of 90% while the latest IPCC AR6 (2022) estimates effective radiative forcing for BC from 1750 to 2019
51 to be $+0.11 (-0.2 \sim +0.42) \text{ W m}^{-2}$. It is important to note that AR5 reported direct radiative forcing while AR6 reports
52 effective radiative forcing. While BC is emitted from nearly all combustion processes, the largest global source of BC
53 is thought to be biomass burning (Bond et al., 2013). Organic aerosol (OA) also absorbs visible light, but its absorption
54 strongly depends on the wavelength of light (Kirchstetter and Novakov, 2004). Non-BC light absorbing organic
55 compounds are often called brown carbon (BrC) and they are usually co-emitted with BC or formed by secondary
56 chemistry in biomass burning plumes (Andreae and Gelencsér, 2006). Unlike BC, which absorbs light from the UV
57 to the IR, BrC absorption sharply increases in the UV and shorter visible portions of the spectrum and has been
58 historically considered to be almost transparent near the red wavelengths (Andreae and Gelencsér, 2006; Bahadur et
59 al., 2012; Liu et al., 2020). The global-mean TOA direct radiative forcing from BrC also shows a large uncertainty,
60 with estimates ranging from $+0.03 \text{ W m}^{-2}$ to $+0.57 \text{ W m}^{-2}$ (Saleh, 2020). Wildfires in the Western U.S. have increased
61 in recent decades (Westerling et al., 2006; Burke et al., 2021), and will continue increasing according to model
62 predictions (Yue et al., 2013; Hurteau et al., 2014; Ford et al., 2018; Neumann et al., 2021). Therefore, quantitative
63 studies of the radiative effects caused by BC and BrC emitted from wildfires are crucial for a better understanding of
64 future climate and essential to improve climate models.

65 The large uncertainty in the radiative forcing from BC is caused both by uncertainties in emissions and by
66 uncertainty in properties that affect its optics, such as size distribution, morphology, refractive index, and mixing state
67 (Bond et al., 2006; Kleinman et al., 2020; Brown et al., 2021). For wildfires, most of the aerosol mass is organic
68 (Garofalo et al., 2019). When BC is internally mixed with OA, the BC is coated by other absorbing or non-absorbing
69 materials that cause more photons to interact with the BC core, and therefore enhance the absorption of the BC core.
70 This process is often called the lensing effect even though geometric lensing is not actually happening at these sizes
71 (Fuller et al., 1999). The absorption enhancement caused by the lensing effect is defined as the ratio of the absorption
72 cross-section of a coated BC particle to that of an equivalent uncoated BC particle (Lack and Cappa, 2010). Laboratory

73 experiments have shown a strong absorption enhancement of BC by a factor of two or more (Schnaiter et al., 2003;
74 Schnaiter et al., 2005; Bond and Bergstrom, 2006; Bond et al., 2006; Peng et al., 2016). Observations of absorption
75 enhancement from ambient BC vary widely in field studies due to variations in coating thickness, coating material,
76 source type, or methodological differences, but it is often much lower than laboratory values (Liu et al., 2015, 2017;
77 Cappa et al., 2012, 2019; Healy et al., 2015; Krasowsky et al., 2016). Cappa et al. (2019) summarized absorption
78 enhancements observed at the red end of the visible spectrum from 10 studies including ambient measurements, source
79 sampling, and lab experiments. The absorption enhancement reported by those measurements ranged from 1.1 to 2.8.
80 Lack et al. (2010) found that the absorption enhancement caused by the absorbing shell would be smaller than the
81 absorption enhancement caused by the pure scattering shell. The non-spherical morphology of BC and the tendency
82 of BC to compact when coated by organics also can both enhance and decrease absorption (Romshoo et al., 2021;
83 Kelesidis et al., 2022).

84 The mass absorption cross section of BC (MAC_{BC}) is an alternative method to quantify the absorbing ability
85 of BC containing particles versus absorption enhancement. By describing the absorption per unit mass of BC, MAC_{BC}
86 can be a fundamental input in climate models to convert mass concentration into absorption coefficients (Cho et al.,
87 2019). MAC_{BC} is the particulate absorption divided by the mass of the pure BC at a certain wavelength. In this way,
88 the calculated MAC_{BC} will include absorption of the BC core along with the absorption and absorption enhancement
89 caused by the coating material. Unfortunately, the MAC of the overall BC particle, MAC_{BC} , in the ambient atmosphere
90 continues to be poorly understood due to a lack of field measurements and limitations of filter-based instruments to
91 measure this parameter. Processes that occur during atmospheric aging of BC also introduce uncertainties in its
92 absorption. Bond and Bergstrom (2006) suggested a MAC_{BC} of $7.5 \pm 1.2 \text{ m}^2 \text{ g}^{-1}$ at 550 nm for fresh BC. The following
93 campaigns demonstrate the variety of MAC_{BC} measured in the ambient during the past 15 years. Subramanian et al.
94 (2010) reported a MAC_{BC} of $10.9 \pm 2.1 \text{ m}^2 \text{ g}^{-1}$ at 660 nm and $13.1 \text{ m}^2 \text{ g}^{-1}$ at 550 nm over Mexico City when using a
95 single particle soot photometer (SP2) and the filter-based particle soot absorption photometer (PSAP) instrument
96 during airborne measurements. Krasowsky et al. (2016) reported a MAC_{BC} enhancement of 1.03 ± 0.05 due to the
97 coatings on BC. Zhang et al. (2017) found a MAC_{BC} with a mean of $10 \text{ m}^2 \text{ g}^{-1}$ and a standard deviation of $4 \text{ m}^2 \text{ g}^{-1}$ at
98 660 nm by using both SP2 and PSAP measurements. Cho et al. (2019) summarized MAC_{BC} estimated from more than
99 10 studies in East and South Asia in both ambient conditions and laboratory experiments, and the values ranged from
100 4.6 to $11.3 \text{ m}^2 \text{ g}^{-1}$.

101 The limitations of current measurement techniques bring major uncertainty into quantifying BrC absorption,
102 because BrC is usually co-emitted with BC which makes it challenging to measure BrC absorption independently.
103 BrC absorption can be directly measured through the solvent-extraction method (Peltier et al., 2007; Zeng et al., 2021;
104 Sullivan et al., 2022) or a thermodenuder (Cappa et al., 2012; Liu et al., 2015; Pokhrel et al., 2017). However, the
105 solvent-extraction method will miss BrC that's insoluble in water or organic solvents, and thermal denuders miss BrC
106 that is not volatile at the denuder temperature. BrC absorption can also be calculated from multi-wavelength total
107 absorption measurements, but this approach must assume the absorption Ångström exponent (AAE) for BC and
108 assumes that BrC does not absorb at longer wavelengths, adding significant uncertainty.

109 To improve understanding of the evolution of light-absorbing aerosol from biomass burning, smoke from 21
110 wildfires in the Western United States were measured near their sources and downwind onboard the NSF/NCAR C-
111 130 aircraft during the Western Wildfire Experiment for Cloud Chemistry, Aerosol Absorption and Nitrogen (WE-
112 CAN) campaign. This campaign represented an airborne attempt to fully characterize Western U.S. wildfires from
113 several different fuel types, locations, and fire stages (flaming vs. smoldering). This paper presents novel observations
114 about the absorbing properties of the aerosol and compares these observations to modeling studies conducted with the
115 WE-CAN data and to results from the Fire Influence on Regional to Global Environment – Air Quality (FIREX) study
116 conducted in 2019 (Zeng et al., 2021).

117 **2 Experimental Method**

118 This work relies on measurements made during the WE-CAN field campaign, which sampled smoke emitted
119 by wildfires across the Western U.S. using the NSF/NCAR C-130 research aircraft. The goal of the campaign was to
120 make detailed observations of the physical, chemical, and optical evolution of aerosol in western wildfire smoke and
121 its impact on climate, air quality, weather, and nutrient cycles. The WE-CAN field campaign consisted of 19 research
122 flights that took place from Jul. 24 – Sep. 13, 2018. Data from 13 flights where all required instrumentation was
123 available were analyzed in this study. The flight path and dominant wildfire for each of these flights are shown in Fig.
124 1. The fire locations, fuel types for each fire during WE-CAN were characterized and summarized by Lindaas et al.
125 (2021).

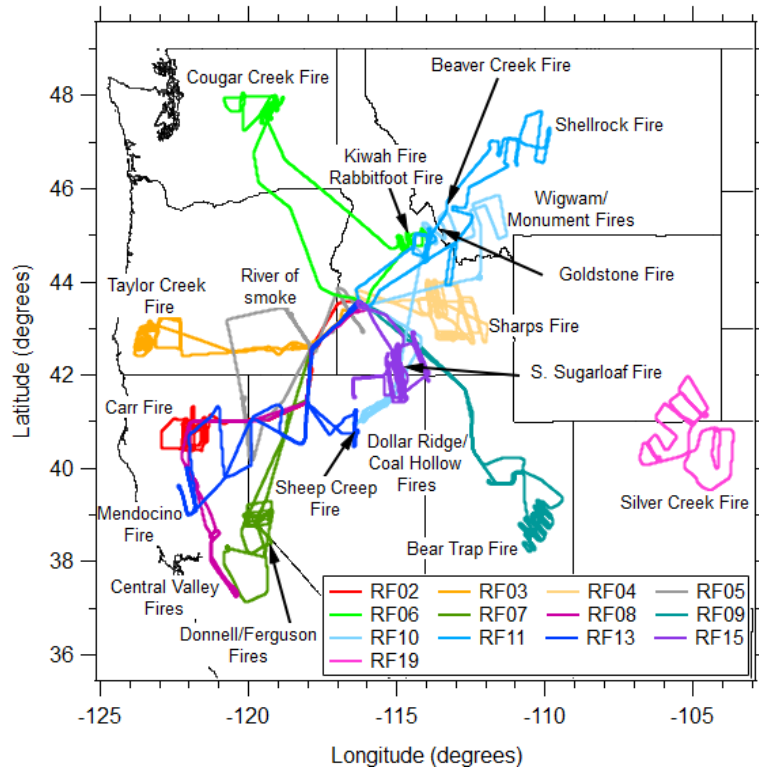


Figure 1: Flight paths and the sampled wildfires for the WE-CAN flights analyzed in this paper.

126 **2.1 Instrumentation**

127 The following instruments are a subset of those flown during the WE-CAN campaign and are utilized in this
 128 work. The full WE-CAN dataset is archived at https://data.eol.ucar.edu/master_lists/generated/we-can. All aerosol
 129 instruments utilized in this paper, except the PILS, pulled air from the same Solid Diffuser Inlet (SDI) inlet. The PILS
 130 sampled from a Submicron Aerosol Inlet (SMAI) (Craig et al., 2013a, 2013b, 2014; Moharreri et al., 2014). To
 131 eliminate artificial differences in the measurements that would arise from different instruments having different
 132 pressures and temperatures after the inlets, all data was converted either to mixing ratio or to STP conditions (1 atm,
 133 0°C). Converting to STP has an additional benefit over converting to ambient conditions in that, similar to mixing
 134 ratio, aerosol mass concentrations ($\mu\text{g m}^{-3}$) and aerosol optical properties (Mm^{-1}) converted to STP stay constant with
 135 altitude unless there is a chemical or physical change beyond parcel expansion. Because of this, conversion to STP
 136 also allows for division of mass concentrations and optical properties by mixing ratios. All the WE-CAN
 137 measurements were converted to standard temperature and pressure (STP, 1 atm, 0°C) based on the measured inlet
 138 temperature and pressure (Eq. 1) before data were uploaded, and they have been used in other papers from WE-CAN
 139 (Palm et al., 2020; Sullivan et al., 2022).

140
$$\text{Variables}_{STP} = \text{Variables}_{measured} \cdot \frac{\text{Pressure}_{STP}}{\text{Pressure}_{measured}} \cdot \frac{\text{Temperature}_{measured}}{\text{Temperature}_{STP}} \quad (\text{Eq. 1})$$

141

142 **2.1.1 Photoacoustic Absorption Spectrometer (PAS)**

143 Aerosol absorption coefficients were measured with the multi-wavelength PAS built by the University of
144 Wyoming (Foster et al., 2019), based on the design of Lack et al. (2012b). A PAS can directly measure the absorption
145 coefficient of dry aerosol. The PAS represents the only way to directly measure aerosol absorption other than a
146 photothermal interferometer (PTI, Sedlacek, 2007), which measures the change in the refractive index of the air near
147 particles caused by heating from absorption. Briefly, when modulated laser light (at the resonant frequency of the cell)
148 is absorbed by the aerosol it heats the surrounding air inducing pressure waves that are amplified by the cavity then
149 detected by two microphones (Lack et al., 2006; Foster et al., 2019). The PAS used here has four cells that measure
150 the aerosol absorption coefficient from dry air at 405 nm and 660 nm and thermally denuded air at 405 nm and 660
151 nm. The denuder was set to 300°C, with the goal of evaporating volatile organic aerosol which might have a potential
152 impact on light absorption. However, absorption from the denuded channels was not used in this study, because the
153 absorption enhancement calculated using the thermodenuder approach was much smaller than the approach taking the
154 ratio of MAC_{BC} to $MAC_{BC-core}$, and we believe the discrepancy is due to the presence of significant residual organic
155 material after denuding. Two NO_x denuders coated with potassium hydroxide, guaiacol and methanol were installed
156 on the PAS in front of the inlet to remove the absorption from gas-phase NO_2 (Williams and Grosjean 1990). No
157 evidence of NO_2 absorption (which would cause baseline shifts) was observed during filter measurements that are
158 acquired every few minutes. A 3 LPM $PM_{2.5}$ cyclone (URG-2000-30ED) was used on the PAS in front of the inlet to
159 provide a $PM_{1.0}$ cut under a total flow rate of 5.7 LPM. In addition, a Nafion drier (Purma Pure PD-100T-24MPS)
160 with 100 tubes was installed on the inlet system to dry sample to a relative humidity below 30%. The particle loss (<
161 3%) in the drier was corrected during post-processing. The uncertainty in the absorption coefficient measured by the
162 PAS mainly comes from the calibration technique, in which the highly absorbing substance Regal Black and the CAPS
163 PM_{SSA} were utilized (Foster et al., 2019). The PAS was routinely calibrated (after each flight or every other day if
164 there was a flight everyday) during WE-CAN with an accuracy of +/- 10%.

165 The PAS microphone shows a pressure-dependent response to pressure. To account for this behavior, we
166 performed pressure-dependent calibration of the PAS where the instrument pressure (both PAS and CAPS PM_{SSA})
167 was dropped stepwise by ~50 torr from ambient to ~300 torr (typical minimum pressure level during WE-CAN). A
168 calibration was performed at each pressure step and the calibration constants were fitted with pressure to get a change
169 in calibration at a desired pressure. Pressure-dependent calibrations were repeated pre and post-campaign to capture
170 variability.

171 **2.1.2 Cavity-Attenuated Phase Shift Spectrometer (CAPS PM_{SSA})**

172 After pulling through the NO_x denuder, the $PM_{1.0}$ cyclone, and the Nafion drier in front of the PAS inlet, the
173 sampled air entered through the Aerodyne CAPS PM_{SSA_450} and CAPS PM_{SSA_660} to measure the aerosol scattering
174 and extinction coefficients at 450 nm and 660 nm, respectively. CAPS PM_{SSA} instruments measure extinction by
175 utilizing the cavity attenuated phase shift spectroscopy and measure scattering with an integrating sphere (Onasch et
176 al., 2015). Ammonium sulfate particles were used to calibrate the scattering channel of the CAPS PM_{SSA} during WE-
177 CAN with an accuracy of +/- 3%.

178 **2.1.3 Particle-into-Liquid Sampler (PILS) systems**

179 BrC absorption and water-soluble organic carbon (WSOC) were measured by a Particle-into-Liquid Sampler
180 (PILS) system (Sullivan et al., 2022). The PILS continuously collects ambient particles into purified water and
181 provides a liquid sample with the aerosol particles dissolved in it for analysis (Orsini et al., 2003). The size-cut for the
182 PILS was provided by a nonrotating microorifice uniform deposit impactor (MOUDI) with a 50% transmission
183 efficiency of 1 μm (aerodynamic diameter) at 1 atmosphere ambient pressure (Marple et al., 1991). The total airflow
184 for the PILS was approximately 15 LPM. Upstream of the PILS was an activated carbon parallel plate denuder
185 (Eatough et al., 1993) to remove organic gases. In addition, a valve was manually closed periodically for 10 min
186 diverting the airflow through a Teflon filter before entering the PILS allowing for background measurements. The
187 liquid sample obtained from the PILS was pushed through a 0.2 μm PTFE liquid filter by a set of syringe pumps to
188 ensure insoluble particles were removed. The flow was then directed through a liquid waveguide capillary cell (LWCC)
189 and Total Organic Carbon (TOC) Analyzer for near real-time measurement of BrC absorption and WSOC,
190 respectively. More details and a schematic illustration can be found in Zeng et al. (2021).

191 For the absorption measurement, a 2.5 m path-length LWCC (World Precision Instruments, Sarasota, FL)
192 was used. A dual deuterium and tungsten halogen light source (DH-mini, Ocean Optics, Largo, FL) and absorption
193 spectrometer (FLAME-T-UV-VIS, Ocean Optics, Largo, FL) were coupled to the LWCC via fiber optic cables.
194 Absorption spectra were recorded using the Oceanview Spectroscopy Software over a range from 200 to 800 nm. The
195 wavelength-dependent absorption was calculated following the method outlined in Hecobian et al. (2010). For this
196 study, a 16 s integrated measurement of absorption with a limit of detection (LOD) of 0.1 Mm^{-1} was obtained (Sullivan
197 et al., 2022).

198 For the WSOC measurement, a Sievers Model M9 Portable TOC Analyzer (Suez Waters Analytical
199 Instruments, Boulder, CO) was used. This analyzer works by converting the organic carbon in the liquid sample to
200 carbon dioxide through chemical oxidation involving ammonium persulfate and ultraviolet light. The carbon dioxide
201 formed was then measured by conductivity. The increase in conductivity observed was proportional to the amount of
202 organic carbon in the liquid sample. The analyzer was run in turbo mode providing a 4 s integrated measurement of
203 WSOC with a LOD of 0.1 $\mu\text{g C/m}^3$ (Sullivan et al., 2022).

204 **2.1.4 Single Particle Soot Photometer (SP2)**

205 Refractory black carbon (rBC) number and mass concentrations were measured with a Single Particle Soot
206 Photometer (SP2; Droplet Measurement Technologies) which uses a continuous, 1064 nm Nd:YAG laser to heat
207 absorbing material, primarily rBC, to its vaporization temperature and measures the resulting incandescence (Schwarz
208 et al., 2006). Similar to the CAPS PM_{SSA} , the sampled air was sent through the NO_x denuder, $\text{PM}_{1.0}$ cyclone, and
209 Nafion drier in front of the PAS inlet before it went to the SP2. The SP2 was calibrated with PSL and size-selected
210 fullerene soot. On the C-130, the SP2 sample line was diluted with HEPA-filtered, pressured ambient air that was
211 passed through a mass flow controller to prevent signal saturation. During post-processing the data was corrected for
212 dilution back to ambient concentrations.

213 **2.1.5 Ultra-High Sensitivity Aerosol Spectrometer (UHSAS)**

214 Particle number concentration was measured by a rack-mounted Ultra-High Sensitivity Aerosol Spectrometer
215 (UHSAS). The flow rate of the rack-mounted UHSAS can be manually lowered by the in-flight operator when the
216 aircraft flew across smoke plumes, so that the UHSAS can stay within its optimum concentration measurement range
217 (Sullivan et al., 2022). The UHSAS was calibrated with ammonium sulfate. The particle mass concentration was
218 calculated by applying these size bins and multiplying by a particle density of 1.4 g cm^{-3} (Sullivan et al., 2022). The
219 volume mean diameter of the particles for all the detected plumes range between $0.18 \text{ }\mu\text{m}$ and $0.34 \text{ }\mu\text{m}$.

220 **2.1.6 Proton-Transfer-Reaction Time-of-Flight Mass Spectrometer (PTR-ToF-MS)**

221 The University of Montana proton-transfer-reaction time-of-flight mass spectrometer (PTR-ToF-MS 4000,
222 Ionicon Analytik) was utilized to report the VOC mixing ratios during WE-CAN (Permar et al., 2021). Only the
223 toluene and benzene mixing ratio derived from the PTR-ToF-MS were used in this work; their overall uncertainty is
224 $< 15\%$. More details of the operation, calibration, and validation on the PTR-ToF-MS during WE-CAN can be found
225 in Permar et al. (2021).

226 **2.1.7 High-Resolution Aerosol Mass Spectrometry (HR-AMS)**

227 Organic aerosol (OA) was detected by the high-resolution aerosol mass spectrometry (HR-AMS; Aerodyne
228 Inc.). The description of the AMS operation during WE-CAN can be found in Garofalo et al. (2019). The atomic
229 oxygen-to-carbon ratios (O:C) and organic mass-to-organic carbon ratio (OM:OC) used in this work were determined
230 via the improved ambient elemental analysis method for the AMS (Canagaratna et al., 2015). Average (integrated)
231 elemental ratios were obtained by averaging (integrating) elemental masses of carbon, hydrogen, and oxygen and
232 recalculating elemental ratios.

233 **2.1.8 Quantum Cascade Laser (QCL) and Picarro Cavity Ring-Down spectrometer (Picarro)**

234 The carbon monoxide (CO) mixing ratio was measured by both an Aerodyne quantum cascade laser
235 instrument (CS-108 miniQCL) and a Picarro cavity ring-down spectrometer (G2401-m WS-CRD) (Garofalo et al.,
236 2019). Because the QCL has better precision than the Picarro instrument, CO measurements from the QCL were
237 preferentially used. However, CO measurements from the Picarro CO data were used for RF10 and RF13, because the
238 CO-QCL was not operated during those two flights. The carbon dioxide (CO_2) mixing ratio was also determined from
239 the Picarro.

240 **2.2 Plume Physical Age**

241 The physical age of the plume was calculated by dividing the distance the plume was sampled from the fire
242 source by the in-plume average wind speed. The average wind speed was measured on the NSF/NCAR C-130 aircraft
243 during each plume pass. The distance was estimated by using the longitude and latitude of the geometric center of the
244 plume measured on the NSF/NCAR C-130 and the fire location provided by the U.S. Forest Service. The same method

245 was used by Garofalo et al. (2019), Peng et al. (2020), Lindaas et al. (2021), Permar et al. (2021), and Sullivan et al.
 246 (2022) and are also utilized here for consistency.

247 **2.3 Plume Integration Method**

248 During the WE-CAN campaign, both the SP2 and PILS had significant hysteresis compared to other
 249 instruments. In the SP2 this is because the sampled air was diluted with particle-free ambient air at various ratios to
 250 prevent signal saturation. In the PILS this is because of the retention effect of liquid on the wetted component or within
 251 dead volumes (Zeng et al., 2021). Therefore, it was most accurate to integrate properties across airborne transects of
 252 wildfire plumes to avoid the impact of instrument hysteresis and measurement noise that can dramatically impact
 253 instantaneous ratios. Pseudo-Lagrangian sampling was used during the flights for the WE-CAN campaign, the C-130
 254 aircraft repeatedly crossed the smoke plume from a particular fire by traveling perpendicular to the prevailing winds,
 255 crossing the plume, turning, then crossing the plume again further downwind. In this work, we manually identified
 256 plume edges based on the inflection point when CO concentrations stopped rapidly changing as we entered and exited
 257 the smoke plume. The outside of plume measurement periods had CO mixing ratios from 100 - 300 ppbv. The lowest
 258 10% of each variable from outside plume segments were set to be the background of that variable. If the time between
 259 two consecutive outside plume segments was larger than 20 s and the highest CO mixing ratio was 100 ppbv higher
 260 than the outside plume CO criteria, this segment was chosen as a plume. The start and end point of each plume was
 261 slightly adjusted manually based on the CO mixing ratio to make sure the entire plume was covered. A different start
 262 and end point for the SP2 and PILS was adjusted manually based on the rBC mass concentrations and WSOC,
 263 respectively.

264 **2.4 Absorption Enhancement and Mass Absorption Cross-section**

265 Absorption enhancement (E_{abs}) is the ratio of the absorption of all particles (including BC core and coating
 266 materials) to the absorption of BC alone (Lack and Cappa, 2010). E_{abs} at 660 nm ($E_{abs,660}$) was calculated in this
 267 study by Eq. 2:

$$268 \quad E_{abs,660} = \frac{Abs_{Total,660}}{M_{BC} * MAC_{BC,core,660}} \quad (Eq. 2)$$

269 where $Abs_{Total,660}$ is the total absorption coefficient at a wavelength of 660 nm measured by the PAS, M_{BC} is the
 270 mass concentration of BC measured by the SP2, and $MAC_{BC,core,660}$ is the MAC of BC alone (without any other
 271 coating material) at 660 nm, which is set to be $6.3 \text{ m}^2 \text{ g}^{-1}$ (Bond and Bergstrom, 2006; Subramanian et al., 2010).

272 MAC_{BC} at 660 nm was calculated following Eq. 3:

$$273 \quad MAC_{BC,660} = \frac{Abs_{Total,660}}{M_{BC}} \quad (Eq. 3)$$

274 $MAC_{BC,660}$ is utilized more often in this study than $E_{abs,660}$ because there is not a widely accepted MAC for
 275 BC emitted from wildfire. MAC of BrC and lensing is calculated at 405 and 660 nm (Eq. 4):

$$276 \quad MAC_{BrC+lensing,\lambda} = \frac{Abs_{Total,\lambda} - M_{BC} * MAC_{BC,core,\lambda}}{M_{OA}} \quad (Eq. 4)$$

277 where M_{OA} is the organic mass measured by the AMS. Again, the $MAC_{BC_core_λ}$ is set to be 6.3 and 10.2 m² g⁻¹,
 278 respectively, at 660 nm and 405 nm yielding an absorption Ångström exponent (AAE, the negative slope of a
 279 logarithmic absorption coefficient against wavelength) of 0.99 for the BC core (Bond and Bergstrom, 2006;
 280 Subramanian et al., 2010; Liu, et al., 2015). It should be noted that both BrC and lensing contribute to the
 281 $MAC_{BrC+lensing_λ}$, and cannot be separated using this approach and $MAC_{BrC+lensing_λ}$ is the MAC of all organics without
 282 distinguishing absorbing and non-absorbing particles.

283 MAC of water-soluble BrC at $λ$ nm ($MAC_{ws_BrCλ}$) is calculated using Eq. 5:

$$284 \quad MAC_{ws_BrCλ} = \frac{Abs_{ws_BrC_λ}}{WSOC * (WSOM:WSOC)} \quad (Eq. 5)$$

285 where $Abs_{ws_BrC_660}$ is water-soluble light absorption and WSOC is water-soluble organic carbon mass, which are
 286 both measured by the PILS system. WSOM:WSOC ratio is set to be 1.6 (Sullivan et al., 2022). $MAC_{ws_BrCλ}$ is the
 287 MAC of all water-soluble organics without distinguishing absorbing and non-absorbing particles.

288 2.5 Fractional non-BC Absorption from BrC

289 Many previous studies of BrC assume that BrC does not absorb significant amounts of light at long
 290 wavelengths (532~705 nm) (Wonaschütz et al., 2009; Lack et al., 2012a; Taylor et al., 2020; Zeng et al., 2021, Zhang
 291 et al., 2022). In this study, a PILS system was used to quantify the absorption of light for water-soluble BrC at 660
 292 nm. This absorption is not likely caused by traditional BC, which is insoluble and will be removed by the PILS
 293 impactor, the 0.2 μm filter in the PILS, and that BC over 110 nm in size will not be oxidized by the TOC analyzer
 294 (Peltier et al., 2007; Zeng et al., 2021; Sullivan et al., 2022).

295 To investigate which contributes more to absorption enhancement at 660 nm, the absorption from BrC or
 296 the lensing effect, the fractional non-BC absorption from BrC at 660 nm is calculated by Eq. 6

$$297 \quad Fractional \ Abs_{BrC} = \frac{Abs_{BrC_660}}{Abs_{Total_660} - M_{BC} * MAC_{BC_core_660}} \quad (Eq. 6)$$

298 where Abs_{Total_660} is the total absorption coefficient at 660 nm which is measured by the PAS, M_{BC} is the mass
 299 concentration of BC which is measured by the SP2, and $MAC_{BC_core_660}$ is the MAC of the BC core at 660 nm which
 300 is set to be 6.3 m² g⁻¹ (Bond and Bergstrom, 2006; Subramanian et al., 2010). Abs_{BrC_660} is the total BrC absorption
 301 coefficient at 660 nm, which is calculated from the water-soluble light absorption provided by the PILS, where we
 302 convert absorption from water-soluble BrC to total BrC. More specifically, to convert the measured light absorption
 303 by water-soluble organics into total BrC absorption in the ambient, it had to be multiplied by two factors. The first
 304 factor converts absorption from water-soluble BrC into absorption from total BrC. This factor is obtained by taking
 305 the ratio between total particulate organic mass and water-soluble particulate organic mass (OM:WSOM). Water-
 306 soluble organic mass is calculated from the PILS WSOC data using a WSOM:WSOC (water-soluble organic mass :
 307 water-soluble organic carbon) ratio of 1.6 (Duarte et al., 2015 & 2019). Ambient organic mass is measured by the
 308 AMS or calculated from the particle size distributions measured by the UHSAS assuming the particle mass all comes
 309 from organic material with a particle density of 1.4 g cm⁻³. Both methods are used and compared in this paper. The
 310 second factor accounts for the fact that particles absorb more light than the same substance in the bulk liquid phase.

311 Here we use Mie theory (Bohren and Huffman, 1983) to convert absorption from BrC in aqueous solution to the
 312 absorption from BrC particles in the ambient (Liu et al., 2013; Zeng et al., 2020). The complex refractive index ($m =$
 313 $n + ik$) was put into a Mie code (implemented into Igor by Ernie R. Lewis base on Bohren and Huffman, 1983) to
 314 obtain the absorption efficiency (Q), and further used to calculate the absorption coefficient by Eq. 7 (Liu et al., 2013).
 315 The real part of the refractive index (n) is set to be 1.55, and the imaginary part is calculated by using Eq. 8 (Liu et al.,
 316 2013).

$$317 \quad Abs(\lambda, D_p) = \frac{3}{2} \cdot \frac{Q \cdot WSOC}{D_p \cdot \rho} \quad (Eq. 7)$$

$$318 \quad k = \frac{\rho \lambda \cdot H_2O_Abs(\lambda)}{4\pi \cdot WSOC} \quad (Eq. 8)$$

319 where λ is the wavelength, D_p is the diameter of the particle, $Abs(\lambda, D_p)$ is absorption coefficient, Q is absorption
 320 efficiency, particle density (ρ) is set to be 1.4 g cm^{-3} , $WSOC$ is the mass concentration of WSOC ($\mu\text{gC m}^{-3}$) measured
 321 by the PILS, and $H_2O_Abs(\lambda)$ is the water-soluble light absorption coefficient measured by PILS. The plume averaged
 322 particle size distribution was used in the calculation, then the absorption coefficient was calculated for each size bin
 323 of UHSAS to obtain the most accurate Mie factor for each plume.

324 The average OM:WSOM factor based on the UHSAS (UHSAS factor) for all the plumes is 2.36 with a
 325 standard deviation is 1.17. The averaged OM:WSOM based on the AMS (AMS factor) is 1.63 with a standard
 326 deviation of 0.74. The average Mie factor at 660 nm is 1.47 (standard deviation of 0.13), which is close to the factor
 327 of 1.36 found by Zeng et al. (2022) based on FIREX data. The Mie factor at 405 nm based on the WE-CAN data is
 328 also calculated, with an average of 1.83, which is similar to the factor that Zeng et al. (2022) determined at 405 nm
 329 (1.7) based on FIREX and Liu et al. (2013) determined at 450 nm (1.9) based on measurements in Atlanta.

330 Sensitivity tests were done on these factors by choosing reasonable ranges of particle density (1.1 g cm^{-3} , 1.4
 331 g cm^{-3} and 1.7 g cm^{-3}) and WSOM:WSOC ratio (1.5, 1.6 and 1.8) (Duarte et al., 2015 & 2019; Finessi, et al., 2012;
 332 Sun et al., 2011) (Table S1). Particle density only affects the Mie factor and UHSAS factor, while WSOM:WSOC
 333 ratio affects the AMS factor and UHSAS factor. As shown in Table S1, the impact of particle density on the Mie factor
 334 (both at 660 nm and 405 nm) is negligible, WSOM:WSOC is the only component that affects the AMS factor (ranging
 335 from 1.48 to 1.73), while the UHSAS factor is much more sensitive (ranging from 1.65 to 3.06) to both particle density
 336 and WSOM:WSOC. Overall, Table S1 demonstrates that none of the factors other than the UHSAS factor are sensitive
 337 to the exact parameters chosen for the calculation, giving confidence that the results presented are robust.

338 This approach assumes that water insoluble BrC has the same refractive index as water soluble BrC. This
 339 assumption would provide a lower estimation on the BrC contribution to the total absorption because Sullivan et al.
 340 (2022) found that 45% of the BrC absorption at 405 nm in WE-CAN came from water-soluble species, and Zeng et
 341 al. (2022) found that insoluble BrC absorbs more at higher wavelengths than soluble BrC, and methanol-insoluble
 342 BrC chromophores caused 87% of the light absorption at 664 nm.

343 2.6 Absorption of BrC and Water-soluble BrC

344 The bulk absorption coefficient of water-soluble BrC at a specific wavelength ($Abs_{ws_BrC\lambda}$) is measured by
 345 PILS system directly. The bulk absorption coefficient of BrC is calculated from Eq. 9:

346 $Abs_{BrC+lensing,\lambda} = Abs_{Total,\lambda} - M_{BC} * MAC_{BCcore,\lambda}$ (Eq. 9)

347 where the $Abs_{Total,\lambda}$ is the total absorption coefficient measured by the PAS. MAC of the BC core is set to
 348 be 6.3 and 10.2 m² g⁻¹, respectively, at 660 nm and 405 nm. It should be noted that both BrC and lensing contribute to
 349 the bulk absorption coefficient, and cannot be separated using this approach.

350 Then the plume integrated absorption and scattering were normalized (x/CO) by taking the ratio of
 351 background-subtracted absorption or scattering (Δx) to the background-subtracted CO mixing ratio (ΔCO) (Eq. 10),
 352 so that the changing of the normalized properties is not impacted by dilution of the plume with background air.

353 $x/CO = \frac{\Delta x}{\Delta CO}$ (Eq. 10)

354 2.7 Modified Combustion Efficiency (MCE)

355 The variation of burn condition (e.g., flaming vs. smoldering) and fuel type can cause a significant difference
 356 in BC emissions and changes in aerosol properties (Akagi et al., 2011; Andreae, 2019). Burn conditions can be
 357 estimated with the modified combustion efficiency (MCE), defined as Eq. 11:

358 $MCE = \frac{\Delta CO_2}{\Delta CO + \Delta CO_2}$ (Eq. 11)

359 where ΔCO_2 and ΔCO are the background-subtracted CO_2 and CO mixing ratio. The background of CO_2 and CO
 360 mixing ratio is obtained via the same process described in Section 2.3.

361 3 Results and Discussion

362 3.1 Comparison of WE-CAN MAC_{BrC} to Modeling Studies

363 It is challenging for climate models to simulate absorption from BrC, especially because it is highly
 364 wavelength dependent and may change with chemical age (Liu et al., 2020). Recently the Saleh et al. (2014)
 365 parameterization has been implemented in models in an attempt to better parameterize the imaginary part of the BrC
 366 refractive index (Wang et al., 2018; Carter et al., 2021). To test how accurately the Saleh parameterization matched
 367 WE-CAN data, the BC:OA ratios measured during WE-CAN were input into the Saleh parameterization, which
 368 provides an imaginary part for the refractive index of BrC ($k_{BrC,\lambda}$) as a function of the BC:OA ratio. The plume
 369 integrated BC:OA ratio for each plume was used in the parameterization, which gave an average k_{BrC} of 0.025, 0.013,
 370 0.009, respectively, at 405 nm, 550 nm and 660nm. Mie theory (Bohren and Huffman, 1983) was then used to calculate
 371 the MAC for BrC. To do the Mie calculations we assumed a real part of the refractive index of 1.7 for BrC (same as
 372 Saleh et al., 2014), used volume mean diameters measured for each plume, and used an organic density of 1.4 g cm⁻³.
 373 Figure 2 compares the observed MAC_{BrC+lensing} (Eq. 4) and MAC_{ws_BrC} (Eq. 5) with the value calculated from the Saleh
 374 parameterization with inputs from WE-CAN. In both the observations and the parameterization, the MAC_{BrC} decreases
 375 as wavelength increases. However, the Saleh parameterization is always significantly larger than the observations.
 376 The MAC_{BrC} from the Saleh parameterization, which does not include lensing effects, is a factor of 3.4 and 2.8 larger
 377 than the observed MAC_{BrC+lensing} at 405 nm and 660 nm, respectively. The range of BC:OA ratios during WE-CAN
 378 (0.007~0.061) is on the very small end of the range (0.005~0.7) used in Saleh's work, and the parameterization failed

379 to capture absorbing aerosol properties for this study. The discrepancy could also be partly because the data Saleh et
 380 al. used for their parameterization comes from controlled laboratory burns and not wildfires or because emissions
 381 observed during WE-CAN have all undergone some near-source aging before being observed by the aircraft. It is
 382 worth noting that the Saleh parameterization of MAC_{BrC} is very sensitive to organic aerosol density. If particle density
 383 is increased from 1.4 g cm^{-3} to 1.7 g cm^{-3} , the Saleh parameterization median MAC_{BrC} decreases to $1.6 \text{ m}^2 \text{ g}^{-1}$ and 0.24
 384 $\text{m}^2 \text{ g}^{-1}$, respectively, at 405 nm and 660 nm (a factor of 2.8 and 2.3, respectively, compared to observed MAC_{BrC} at
 385 405 nm and 660 nm). The fact that the Saleh parameterization overestimates the absorption property of biomass aerosol
 386 especially for fresh emitted aerosols suggests that different parameterizations are needed for the Western U.S.. Carter
 387 et al. (2021) utilized the Saleh parameterization for BrC absorption in the GEOS-Chem model and also found that the
 388 Saleh model overestimated BrC absorption for WE-CAN. It was hypothesized that the overestimation was due to the
 389 lack of a bleaching process for BrC in the model and offset part of the overestimation by bringing in bleaching into
 390 the model.

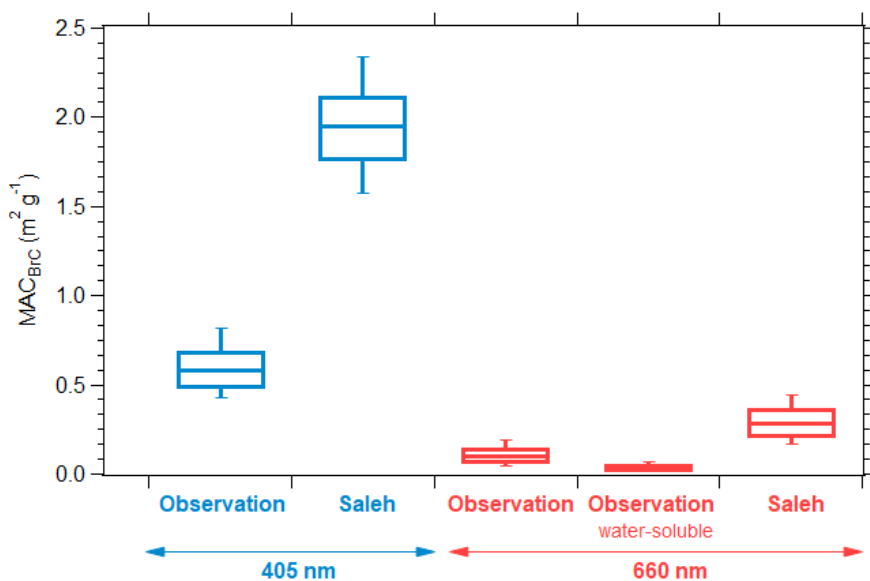


Figure 2: Boxplot summary for observed and parameterized (Saleh) MAC_{BrC} at 405 nm (blue) and 660 nm (red). For each box, the central line represents the median, the top and bottom edges represent the 75th and 25th percentile, and the top and bottom whiskers represent the 90th and 10th percentile of the data.

391 3.2 Investigation of BrC Bleaching at Visible Wavelengths

392 A limited number of field measurements have shown BrC decay with chemical age (Forrister et al., 2015;
 393 Wang et al., 2016). Despite a relatively poor understanding of the mechanism of bleaching or whitening of BrC, this
 394 process has been implemented in numerous model simulations (Brown et al., 2018; Wang et al., 2018; Carter et al.,
 395 2021). While only a fraction of organic aerosol mass absorbs light, both models and observations typically treat all
 396 organics as equally absorbing because of the inability to distinguish absorbing and non-absorbing molecules. The
 397 definition of bleaching or whitening was unclear in previous literature. Models tend to treat bleaching as the change
 398 of refractive index or decreasing of MAC (Brown et al., 2018; Wang et al., 2018; Carter et al., 2021), while
 399 observations or lab experiments mostly link bleaching to the decrease of normalized total absorption (Forrister et al.,

2015; Palm et al., 2020; Zeng et al., 2022). It is important to distinguish between these two, because the decrease of absorption coefficient can also be caused by loss of absorbing organic material, which will also change the scattering coefficient and radiative forcing. Therefore, the MAC of BrC and the absorption coefficient of BrC at visible wavelengths were calculated and analyzed together with two chemical clocks (O:C and toluene:benzene ratio) and organic mass, to determine whether BrC bleached during the WE-CAN campaign, and whether the bleaching was caused by the less organic mass or the changing of refractive index. Because all large wildfire emissions are a mix of different regions that are burning slightly different fuels at different combustion efficiencies and because models treat regions, not individual fires, we identify relationships in this paper that hold true across all the flight data collected during WE-CAN. These types of broad correlations are much more useful than individual case studies yielding results that only hold true sometimes.

3.2.1 Consistency of The Mass Absorption Cross-Section of BrC at 405 nm

Palm et al. (2020) combined data from WE-CAN and the Monoterpene and Oxygenated aromatic Oxidation at Night and under LIGHTs (MOONLIGHT) chamber experiment and found that evaporated biomass-burning POA is the dominant source of biomass-burning SOA in wildfire plumes during the first a few hours after emission. They also found that of the SOA formed from oxidation, phenolic compounds contribute $29 \pm 15\%$ of BrC absorption at 405 nm. In this section, we analyze the characteristics of BrC at 405 nm to understand the average properties of BrC and to understand the balance of BrC formation versus bleaching during WE-CAN. The MAC of BrC is calculated following Eq. 4 and therefore it includes a contribution from the lensing effect. The MAC of water-soluble BrC is calculated following Eq. 5. Figure 3 shows the MAC of BrC at 405 nm versus the aerosol oxidation level (O:C ratio), while Fig. S2 is a similar plot that uses a simple photochemical clock, the gas-phase toluene:benzene ratio. The O:C ratio characterizes the oxidation state of OA and typically increases with photochemical age (Aiken et al., 2008), while the toluene:benzene ratio decreases with photochemical processing time since toluene is more reactive than benzene (Gouw et al., 2005). Both markers are two commonly used markers to indicate the chemical age of smoke, and they correlated well with each other during WE-CAN (Fig. S1).

The $MAC_{BrC+lensing_405}$, varies from $0.08 \text{ m}^2 \text{ g}^{-1}$ to $1.6 \text{ m}^2 \text{ g}^{-1}$ with a mean value of $0.59 \text{ m}^2 \text{ g}^{-1}$ and a standard deviation of 0.19. The largest values are from RF05, the flight through California, Oregon, and Idaho, where aged smoke from different fires was mixed. The large $MAC_{BrC+lensing_405}$ occurred when the aircraft left the smoke-filled boundary layer during RF05. If we exclude $MAC_{BrC+lensing_405}$ from RF05, the values range from $0.08 \text{ m}^2 \text{ g}^{-1}$ to $1.09 \text{ m}^2 \text{ g}^{-1}$, but still have a mean value of $0.59 \text{ m}^2 \text{ g}^{-1}$ and a standard deviation of 0.15. Again, we note that this value includes the contribution of lensing. Despite this, our results lie in the same range as those measured without the contribution of lensing of $0.31 \pm 0.09 \text{ m}^2 \text{ g}^{-1}$ measured in CLARIFY-2017 (Taylor, 2020), $0.13\text{-}2.0 \text{ m}^2 \text{ g}^{-1}$ measured in FIREX-AQ (Zeng et al., 2022), and $0.25\text{-}1.18 \text{ m}^2 \text{ g}^{-1}$ measured in ORACLES (Zhang et al., 2022). Very weak or non-trends are observed versus the chemical markers of aging (Fig. 3). If there is any trend, it is a slight increase in MAC_{ws_BrC405} with O:C ratio with a poor correlation. A similar weak trend is also observed when compared MAC_{ws_BrC405} and $MAC_{BrC+lensing_405}$ with the toluene:benzene ratio (Fig. S2). The flat or slightly increasing trend with increasing oxidation level and decreasing toluene:benzene suggests that the refractive index of BrC is not changing in

436 a consistent way at 405 nm. It is important to remember that most of the trends observed in WE-CAN are caused by
 437 emissions from different fires versus variations within a single fire, which tend to be quite small. Only 2 flights shows
 438 a clear trend ($R^2 > 0.3$) for both MAC_{ws_BrC405} and $MAC_{BrC+lensing_405}$ with increasing O:C ratio at the same time, and
 439 they are RF03 (R^2 of 0.85 and 0.85 with positive slope for MAC_{ws_BrC405} and $MAC_{BrC+lensing_405}$), and RF06 (R^2 of 0.8
 440 and 0.49 with negative slope for MAC_{ws_BrC405} and $MAC_{BrC+lensing_405}$), where RF03 only measured a single fire (Taylor
 441 Creek fire).
 442

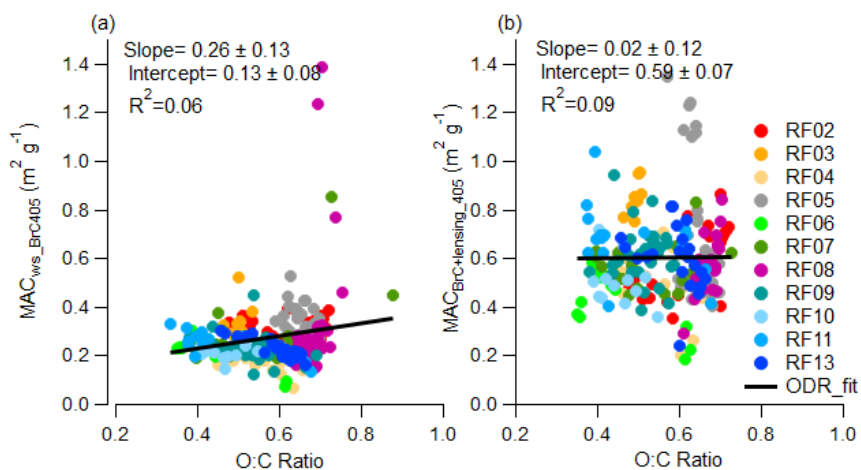


Figure 3: Plume integrated (a) MAC_{ws_BrC405} and (b) $MAC_{BrC+lensing_405}$ variations with the organic aerosol O:C ratio

443 RF05 and RF08 were chosen as case studies, to observe the optical properties of highly aged aerosol to see
 444 if the optical properties of this aerosol were similar to those observed in the near-field plume sampling of individual
 445 fires at the longest chemical or physical age observed, which was roughly 6-24 hours of physical aging. RF08 was a
 446 flight through the Central Valley of California where aged smoke from multiple fires that had settled into the valley
 447 was measured while RF05 was a flight in which smoke from several California fires was observed in California,
 448 Oregon and Idaho roughly 300~600 miles from the fires (flightpaths are shown in Fig. 1). $MAC_{BrC+lensing_405}$, CO
 449 mixing ratio, toluene:benzene ratio, and O:C ratio are displayed in Fig. 4a and 4b. The mixing ratio of CO is relatively
 450 low in these aged dilute smoke plumes vs. the plumes near the sources analyzed earlier. 1-minute averages of
 451 $MAC_{BrC+lensing_405}$ are calculated to reduce noise and 1-minute-averages for toluene:benzene ratio and O:C ratio were
 452 calculated and all the negative values were removed. As shown in Fig. 4, the smallest toluene:benzene ratio is ~0.35
 453 in RF05, and is ~0.16 in RF08, while the largest O:C ratio is ~0.7 in both RF05 and RF08, which indicates these two
 454 cases indeed captured plumes that appear chemically aged to similar extent to the other near-source flights where the
 455 smallest toluene:benzene ratio was 0.33 and the largest O:C ratio was 0.88 in near-fire measurements (Fig. 3, Fig. S2,
 456 and Fig S6a).

457 In RF05 (Fig. 4a), the weighted average O:C ratio over the entire flight was 0.64, and the toluene:benzene
 458 ratio averaged 0.45 with a standard deviation of 0.05. $MAC_{BrC+lensing_405}$ varied from $0.36 \text{ m}^2 \text{ g}^{-1}$ to $1.52 \text{ m}^2 \text{ g}^{-1}$ with an
 459 average of $0.66 \text{ m}^2 \text{ g}^{-1}$ and a standard deviation of $0.26 \text{ m}^2 \text{ g}^{-1}$. The plume that was measured in this flight was a
 460 mixture of different fire sources. Despite the much longer transit time and distance, overall these emissions, which

461 were measured 300 to 600 miles away, have a very similar $MAC_{BrC+lensing_405}$ to that of the near-source flights where
 462 we tracked emissions from as near to the fire source as allowed by air traffic control.

463 The RF08 (Fig. 4b) results are similar to RF05, even though these emissions were smoke of mixed aged from
 464 multiple fire sources in the Central Valley of California. The weighted average O:C ratio was 0.67 over the entire
 465 measurement, and average toluene:benzene ratio was 0.41 with a standard deviation of 0.15. $MAC_{BrC+lensing_405}$
 466 averaged $0.59 \text{ m}^2 \text{ g}^{-1}$ with a standard deviation is $0.14 \text{ m}^2 \text{ g}^{-1}$. There are several extreme values that exist in the dataset,
 467 probably because of the SP2 hysteresis caused by variation in the dilution rate of the SP2 which cannot be totally
 468 eliminated from the 1-minute average. In addition, the smoke from RF08 (Fig. 4b) is split into four regions based on
 469 varying observed CO mixing ratios, and integrated $MAC_{BrC+lensing_405}$ is calculated for each region (purple star marker).
 470 The regional edges are represented by blue dashed lines. Integrated $MAC_{BrC+lensing_405}$ for all of these variable CO
 471 regions is relatively stable with an average value of $0.59 \text{ m}^2 \text{ g}^{-1}$ and a standard deviation of $0.07 \text{ m}^2 \text{ g}^{-1}$.
 472

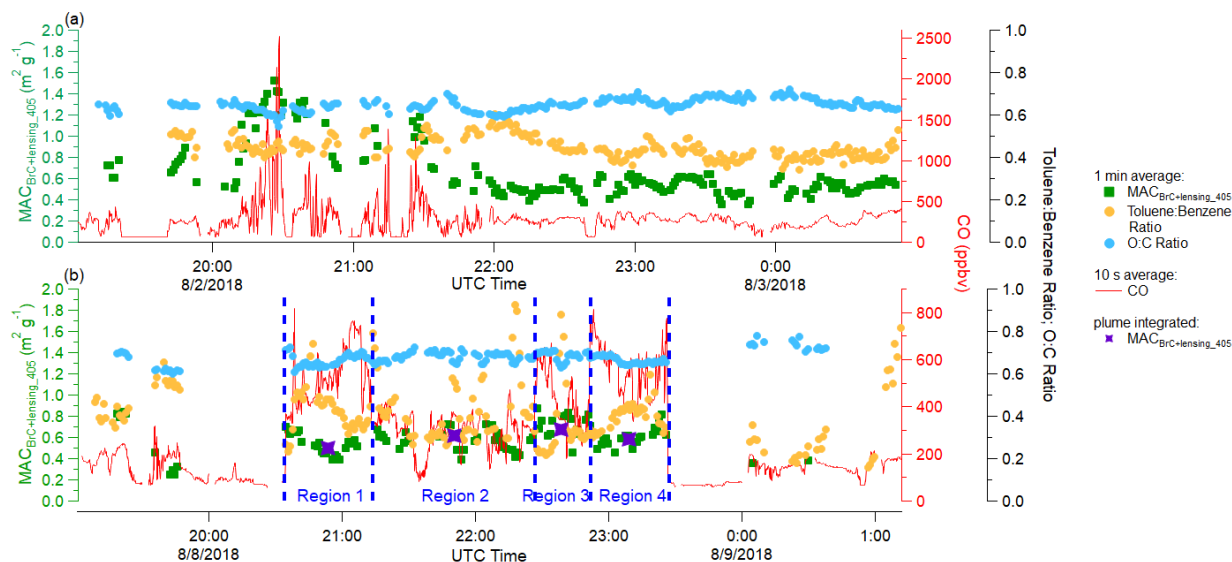


Figure 4: Time series of plume properties during (a) RF05 (measurements far from fire source), and (b) RF08 (Central Valley of California). Different square and round markers indicate 1 min averages of different variables as shown in the legend, and the red solid line represents 10 s averages of the mixing ratio of CO. Purple stars in RF08 indicate region integrated $MAC_{BrC+lensing_405}$ (individual regions are separated based on the concentration of CO, and indicated by blue dashed lines).

473 3.2.2 Decrease in Absorption at 405 nm Observed with Markers of Chemical Oxidation

474 Although neither the $MAC_{BrC+lensing_405}$ nor MAC_{ws_BrC405} decreases with O:C or Toluene:Benzen, Fig. 5
 475 shows that BrC bleaching is observed in terms of decreased total absorption. Figure 5a and 5c show the behavior of
 476 BrC absorption at 405 nm with markers of the aerosol oxidation level (O:C) and photochemistry (toluene:benzene).
 477 The absorption coefficient of BrC shown in Fig. 5 is calculated by Eq. 9-10, which cannot separate the absorption
 478 caused by the BrC and lensing effect. To confirm that observed trends are not the result of changing lensing, the
 479 absorption coefficient of water-soluble BrC measured by the PILS, which does not include lensing effects, is also
 480 compared in Fig. 6a and 6c. The average water-soluble BrC absorption at 405 nm (Abs_{ws_BrC405} , $0.02 \text{ Mm}^{-1} \text{ ppbv}^{-1}$)

481 which is directly measured by the PILS, is only 20% of the total absorption from BrC plus lensing ($Abs_{BrC+lensing_405}$,
482 $0.11 \text{ Mm}^{-1} \text{ ppbv}^{-1}$), which is calculated from the PAS and SP2 (Eq.9). However, $Abs_{BrC+lensing_405}$ and Abs_{ws_BrC405}
483 both decrease with increasing O:C ($R^2 = 0.65$ and $R^2 = 0.3$, respectively for $Abs_{BrC+lensing_405}$ and Abs_{ws_BrC405}) and
484 decreasing toluene:benzene ratio, which suggest a similar level of decreasing BrC absorption for all the fires observed
485 in WE-CAN from numerous locations in the western U.S.. This relationship holds despite differences in fuel type,
486 burn conditions, meteorology, etc. between all of these fires. The observed trends are mostly due to the decreasing of
487 both total OA mass (Fig. 5b and 5d) and WSOC (Fig. 6b and 6d) with the increasing O:C ratio ($R^2 = 0.8$ and $R^2 = 0.4$,
488 respectively for OA and WSOC) and decreasing toluene:benzene ratio ($R^2 = 0.64$ and $R^2 = 0.44$, respectively for OA
489 and WSOC). Overall, the organic aerosol O:C ratio better predicts BrC evolution than toluene:benzene ratio, probably
490 because it is a particle-phase property rather than a gas-phase one. Again, it is important to clarify if BrC “bleaching”
491 is caused by decreasing BrC absorption coefficient or decreasing of BrC refractive index (or MAC). In this study,
492 decreasing MAC_{BrC} is not observed, rather the BrC absorption coefficient decreases significantly with the the simple
493 O:C and Toluene:Benzene chemical clocks due to loss of OA mass. Less OA mass also causes decrease in bulk
494 scattering coefficient (Fig. S3), leading to a very different net radiative effect than reducing MAC_{BrC} .

495 It is important to recall that we aimed to find general trends that hold for all fires in the western U.S., and the
496 above trend is significant when all fires are grouped together, although the trend is, in fact, not robust in each flight
497 and is rather due to variations between the fire plumes rather than variation within a single fire plume. Figure 7 shows
498 the correlation between normalized OA and chemical age for each fire source. It demonstrates that different fires show
499 different relationships and that OA does not always decrease with oxidation level/chemical aging within a single fire
500 (Kiwah fire and Rabbitfoot fire), though increasing O:C ratio does correlate well ($R^2 > 0.3$) with decreasing OA mass
501 in 7 fires (with R^2 of 0.94 for Taylor Creek fire, 0.87 for Carr fire, 0.86 for Beaver Creek fire, 0.8 for Coal Hollow
502 fire, 0.76 for Bear Trap fire, 0.35 for Sharps fire, and 0.31 for Sugarloaf fire). Toluene:benzene ratio didn't track OA
503 as good as O:C ratio, and decreasing toluene:benzene ratio correlates well ($R^2 > 0.3$) with decreasing OA mass in 3
504 fires (with R^2 of 0.87 for Rabbitfoot fire, 0.85 for Coal Hollow fire, and 0.84 for Bear Trap fire).

505

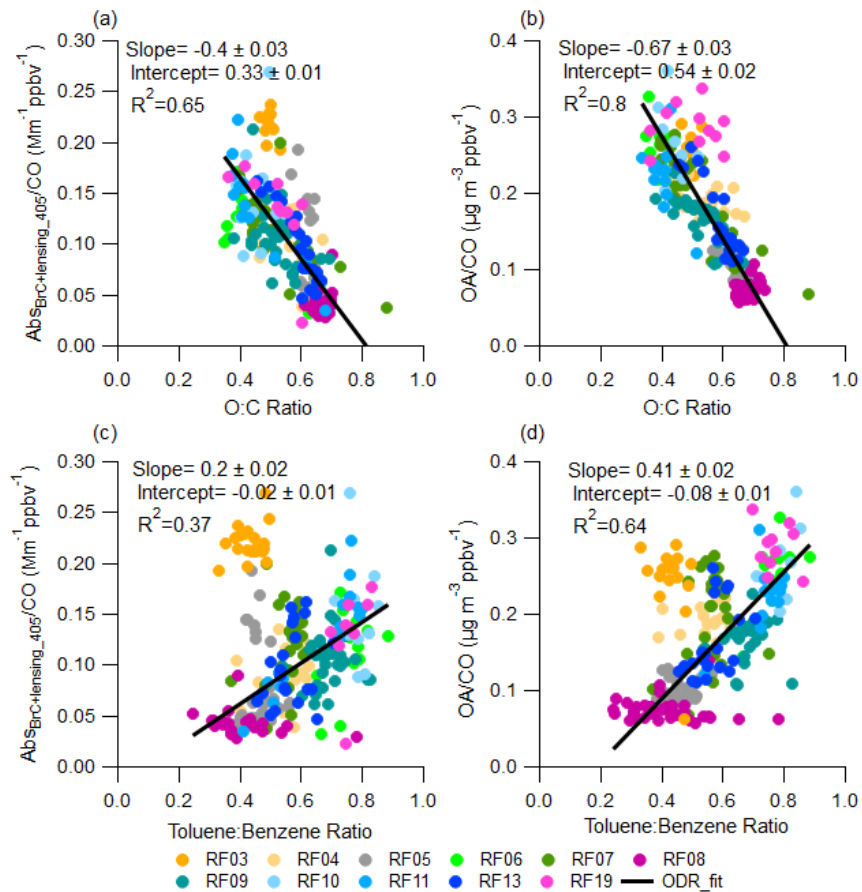


Figure 5: Plume integrated normalized $Abs_{BrC+lensing_405}$, and OA variation with chemical age. Top panels show (a) plume integrated normalized $Abs_{BrC+lensing_405}$, and (b) plume integrated normalized OA variation with O:C ratio. Bottom panels show (c) plume integrated normalized $Abs_{BrC+lensing_405}$, and (d) plume integrated normalized OA variation with toluene:benzene ratio. Data from RF03 was excluded from the ODR fit with toluene:benzene ratio, because RF03 sampled the injection of fresh smoke into the free troposphere, where gas species reacted more rapidly than particles and toluene:benzene ratio failed to keep track of aerosol evolution.

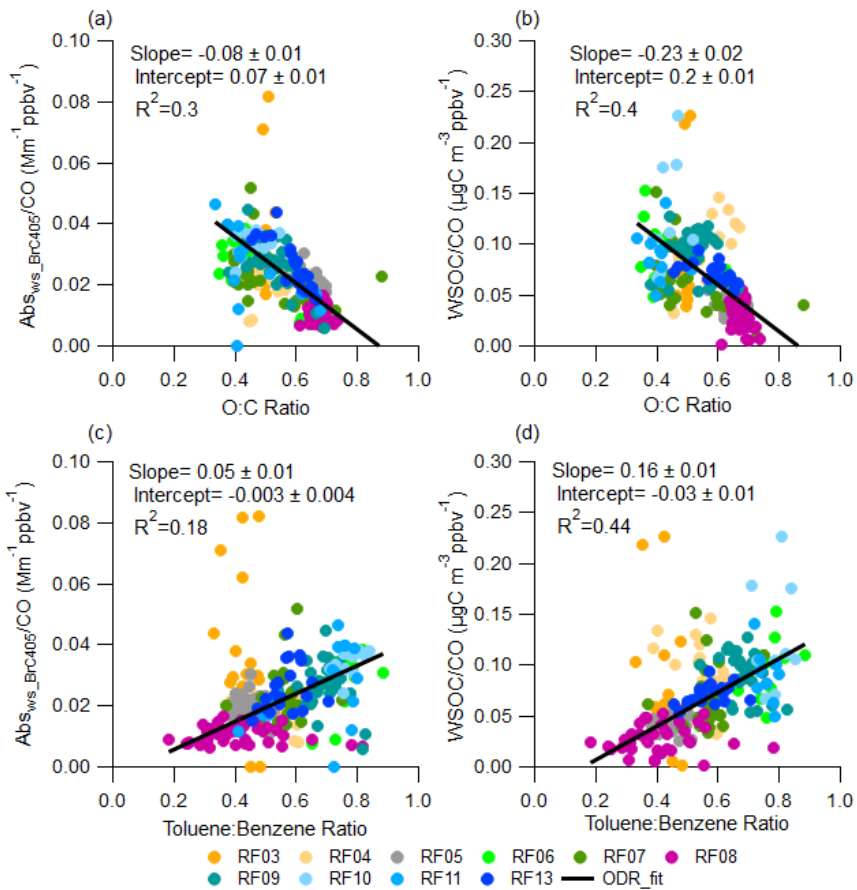


Figure 6: Similar to Fig. 5, but with plume integrated normalized Abs_{ws_BrC405} , from PILS in (a) and (c), and WSOC in (b) and (d)

507

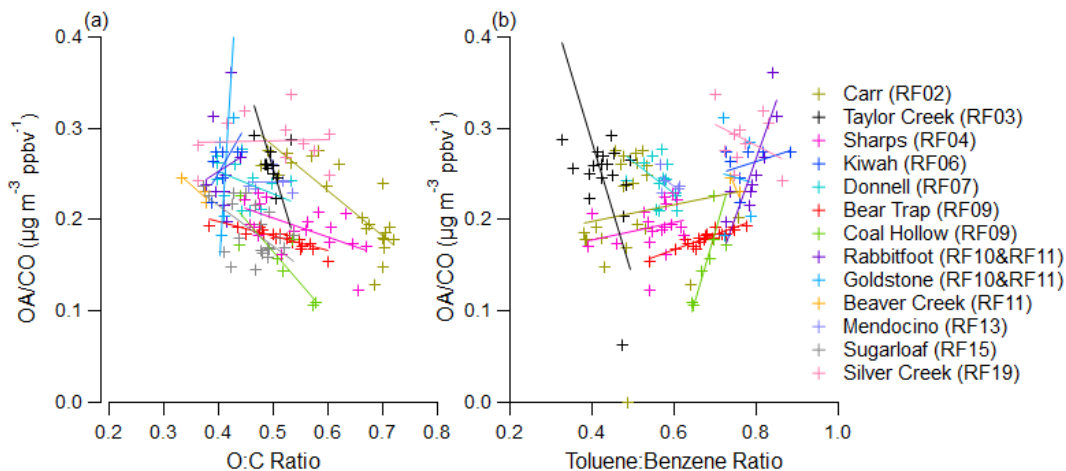


Figure 7: Plume integrated normalized OA variation with (a) $O:C$ ratio and (b) toluene:benzene ratio. Different colors were used to distinguish plumes from different fire sources. Plumes from uncertain fire sources (especially plumes from RF05, RF08) were not included in this plot.

508

509 No trend is observed in CO normalized OA mass with plume physical age (Fig. S4), which is consistent with
510 the result from Garofalo et al. (2019) in that no net OA mass change was observed in individual plumes during WE-
511 CAN when they are characterized by physical age, although more data from additional fires were included in the
512 current work. Plume-integrated CO-normalized OA also shows weak or no trend with altitude and temperature (Fig.
513 S5). However, we note that the smallest OA:CO was captured in the plumes (RF08) that have highest temperature
514 (~305 K), and larger OA:CO tends to be observed in the colder plumes (RF19). More studies are needed to determine
515 how much OA is evaporated in high temperature plumes because the WE-CAN dataset does not capture enough
516 variation of temperature within plumes to make a robust conclusion. No clear trend was found between
517 $MAC_{BrC+lensing_405}$ and physical age or MCE (Fig. S6). Similar behavior was also observed in Western wildfires at 405
518 nm in FIREX-AQ (Zeng et al., 2022). Part of the reason is that for most fires, we only captured the first few hours (<
519 15 h), and MCE do not have a robust capability to predict biomass burning particle properties (McClure et al., 2020).
520 No trend is found between $MAC_{BrC+lensing_405}$ and altitude or temperature (Fig. S7). The trend with BC:OA ratio (Fig.
521 S8) is not as clear as in Saleh et al. (2014), most probably because the range of BC:OA ratios observed during WE-
522 CAN (0.007~0.061) is much smaller than that (0.005~0.7) observed in Saleh's work. Even in their work, the increasing
523 trend is not very clear if one only focuses on the region where the BC:OA ratio is less than 0.03. Also, the Saleh et al.
524 (2014) results were obtained from laboratory burns and not wildfires, which might also cause a discrepancy.

525 3.2.3 Mass Absorption Cross-Section and Optical Properties of BrC at 660 nm

526 BrC is defined as OA that has strong absorption at UV and shorter visible portions of the spectrum and has
527 been historically considered to be almost transparent near the red wavelengths (Andreae and Gelencsér, 2006; Bahadur
528 et al., 2012; Liu et al., 2020). However, during WE-CAN, we were able to quantify Abs_{ws_BrC660} with the PILS
529 instrument. We know that absorption observed in the PILS at 660 nm is not BC because BC is insoluble and will be
530 removed by the PILS impactor, the 0.2 μm filter in the instrument, and that BC over 110 nm in size will not be oxidized
531 by the TOC analyzer (Peltier et al., 2007; Zeng et al., 2021; Sullivan et al., 2022). Next, we investigate the behavior
532 of BrC absorption at 660 nm to see if BrC has a similar behavior at the long versus short ends of the visible spectrum.

533 Figure 8 shows the behavior of brown carbon at 660 nm vs. the O:C ratio. Similar to 405 nm, no bleaching
534 in terms of decreased MAC is observed at 660 nm. If there is any trend, it is increasing MAC_{ws_BrC660} and
535 $MAC_{BrC+lensing_660}$ with organic aerosol O:C ratio. Similar trends are observed, though with lower correlation, versus
536 the toluene:benzene ratio (Fig. S9). The mean value of $MAC_{BrC+lensing_660}$ is $0.11 \text{ m}^2 \text{ g}^{-1}$ (with a standard deviation of
537 0.06), which is much larger than the 0.03 average of MAC_{ws_BrC660} , a result we have attributed to the lensing effect,
538 but which could also partially be the result of water-insoluble BrC having a higher MAC than water-soluble BrC.

539 These results for the behavior of MAC_{BrC} at different wavelengths derived using different instruments (PAS
540 and PILS) is further evidence that MAC_{BrC} does not decrease with physical or chemical age in the WE-CAN dataset.
541 At a minimum, the plume integrated results, which represent total optical properties relevant to climate models, do
542 not capture any MAC_{BrC} decay that might be occurring at the edges of the plume.

543

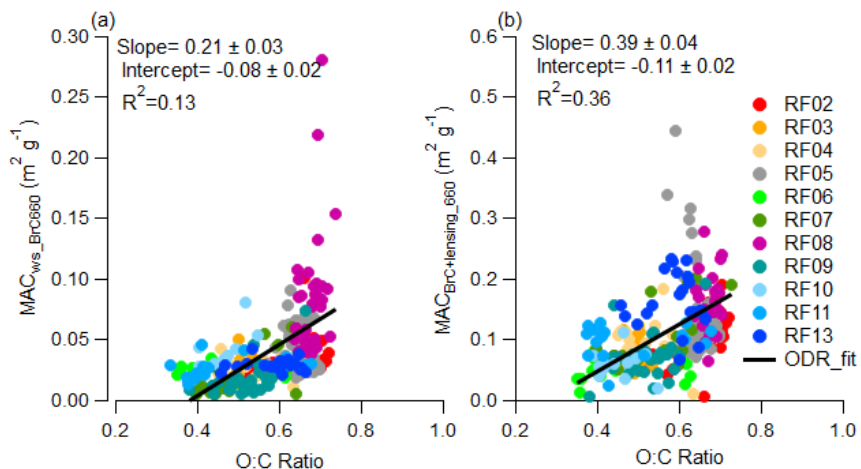


Figure 8: Plume integrated (a) MAC_{ws_BrC660} and (b) $MAC_{BrC+lensing_660}$ variations with O:C ratio

544 Similar to our analysis at 405 nm, RF05 and RF08 are presented as case studies to investigate the behavior
 545 of $MAC_{BrC+lensing_660}$ in aged plumes emitted from different fire sources. Figure 9 is similar to Fig. 4, but with
 546 $MAC_{BrC+lensing_660}$ instead of $MAC_{BrC+lensing_405}$. For the case of RF05 (Fig. 9a) $MAC_{BrC+lensing_660}$ varied from 0.04 m^2
 547 g^{-1} to $0.40 \text{ m}^2 \text{ g}^{-1}$ with an average of $0.15 \text{ m}^2 \text{ g}^{-1}$ and a standard deviation of $0.07 \text{ m}^2 \text{ g}^{-1}$. The $MAC_{BrC+lensing_660}$ tends
 548 to be larger when CO mixing ratio is higher, but does not have a significant correlation with any marker of oxidation
 549 level or photochemistry shown in Fig. 9. For the case of RF08 (Fig. 9b) $MAC_{BrC+lensing_660}$ is more stable than in RF05,
 550 and varied from $0.04 \text{ m}^2 \text{ g}^{-1}$ to $0.37 \text{ m}^2 \text{ g}^{-1}$ with an average of $0.18 \text{ m}^2 \text{ g}^{-1}$ and a standard deviation of $0.06 \text{ m}^2 \text{ g}^{-1}$. The
 551 regional integrated $MAC_{BrC+lensing_660}$ is even more stable with an average value of $0.16 \text{ m}^2 \text{ g}^{-1}$ and a standard deviation
 552 of $0.01 \text{ m}^2 \text{ g}^{-1}$. Similar to the results at 405 nm, we observe that the MAC in these very aged plumes is very similar to
 553 the average MAC observed in the near field.
 554

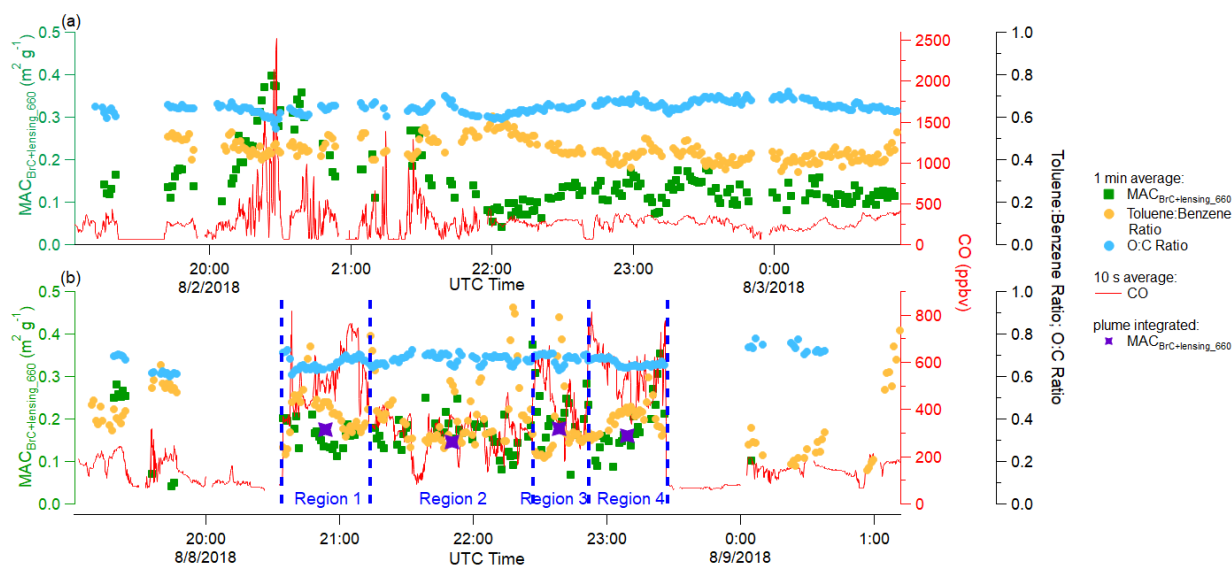


Figure 9: Time series of plume properties during (a) RF05, and (b) RF08(Central Valley of California). Different square and round markers indicate 1 min averages of different variables as shown in the legend, and the red solid line represents 10 s averages of the mixing ratio of CO. Purple stars in RF08 indicate region integrated $MAC_{BrC+lensing_660}$ (individual regions are separated based on the concentration of CO, and indicated by blue dashed lines).

555 Normalized $Abs_{BrC+lensing_660}$ and total scattering coefficient at 660 nm (Fig. S10), as well as normalized
 556 Abs_{ws_BrC660} (Fig. S11) were also investigated to see if they decreased with markers of chemical age similar to the
 557 results seen at 405 nm. However, the correlation between these BrC optical properties with O:C ratio or
 558 toluene:benzene ratio at 660 nm is much weaker and flatter than they are at 405 nm. Perhaps this is because BrC
 559 absorption is very small at 660 nm, and a large uncertainty is brought in from the assumptions required for calculation
 560 of this property and instrumental uncertainties. The average normalized $Abs_{BrC+lensing_660}$ is $0.02 \text{ Mm}^{-1} \text{ ppbv}^{-1}$, which
 561 is 5 times lower than the absorption at 405 nm; while the average normalized Abs_{ws_BrC660} is a order of magnitude
 562 lower than Abs_{ws_BrC405} . The $MAC_{BrC+lensing_660}$ (Fig. S12) shows better correlation with BC:OA ratio than
 563 $MAC_{BrC+lensing_405}$, though the increasing trend is still not as significant as Saleh et al. (2014) due to a much smaller
 564 BC:OA ratio during WE-CAN.

565 3.3 Relative Importance of BrC vs. the Lensing Effect at 660 nm

566 Plume integrated MAC_{BC} at 660 nm (MAC_{BC660}) from the 13 WE-CAN research flights with clear plume
 567 transects of biomass burning plumes are shown in Fig. 10. The MAC_{BC660} discussed in this section is calculated from
 568 Eq. 3, and has contributions from absorption from the BC core, the BrC shell, and the lensing effect. Again, even fire
 569 plumes from individually named fires are usually a mix of many different burning conditions, and it is hard to identify
 570 the exact source in most wildfire smoke measurements, especially for well mixed plumes. Therefore flight-to-flight
 571 data is analyzed because each flight covered a region, and an overall behavior of absorbing aerosol from wildfire can
 572 be provided. MAC_{BC660} varies between different flights with RF03 having the highest average MAC_{BC660} of 12.9 m^2
 573 g^{-1} , and RF10 having the lowest average MAC_{BC660} of $8.6 \text{ m}^2 \text{ g}^{-1}$. Even in highly aged plumes with emissions mixed
 574 from multiple fires (RF05 and RF08), the MAC_{BC660} is similar in magnitude and consistency with an average of 11.3

575 $\pm 1.8 \text{ m}^2 \text{ g}^{-1}$. The average of all plume-integrated $\text{MAC}_{\text{BC660}}$ is $10.9 \text{ m}^2 \text{ g}^{-1}$, with a standard deviation of $2.1 \text{ m}^2 \text{ g}^{-1}$.
 576 This result is similar to some other recent airborne measurements. Subramanian et al. (2010) reported a $\text{MAC}_{\text{BC660}}$ of
 577 $10.9 \pm 2.1 \text{ m}^2 \text{ g}^{-1}$ using a SP2 and PSAP operated during the MILAGRO campaign, which included airborne
 578 measurements of biomass burning over Mexico. Similarly, Zhang et al. (2017) estimated a $\text{MAC}_{\text{BC660}}$ of $10 \text{ m}^2 \text{ g}^{-1}$
 579 utilizing both SP2 and PSAP deployed on the NASA DC-8 research aircraft for the DC3 campaign, which measured
 580 the upper tropospheric BC over the central U.S. Taylor et al. (2020) calculated a $\text{MAC}_{\text{BC655}}$ of $12 \pm 2 \text{ m}^2 \text{ g}^{-1}$ for biomass
 581 burning emissions from Africa over the southeast Atlantic Ocean, using airborne measurements from a SP2 and PAS
 582 in the CLARIFY-2017 campaign.

583 These results are encouragingly similar given the breadth of measurement techniques (PSAP is filter-based
 584 whereas PAS is a direct measurement), geographic regions (Continental U.S. for DC3, Mexico for MILAGRO, African
 585 outflow for CLARIFY) and altitude in the atmosphere (all were airborne campaigns covering a range of altitudes). If
 586 we apply $6.3 \text{ m}^2 \text{ g}^{-1}$ as the MAC of a BC core at 660 nm (Bond and Bergstrom, 2006; Subramanian et al., 2010), then
 587 the average absorption enhancement for the entire WE-CAN campaign is 1.7. This means the absorption of coated BC
 588 is 1.7 times higher than bare BC at 660 nm, which is somewhat close to the factor of ~ 2 reported by laboratory
 589 experiments (Schnaiter et al., 2005; Peng et al., 2016), larger than some field measurements (Cappa et al., 2012&2019;
 590 Healy et al., 2015), but close to 1.85 ± 0.45 measured by Taylor et al. (2020) in African biomass burning plumes. The
 591 similarity to the Taylor et al. (2020) result suggests global similarities in the $\text{MAC}_{\text{BC660}}$ from aerosol emitted from
 592 wildfires.

593

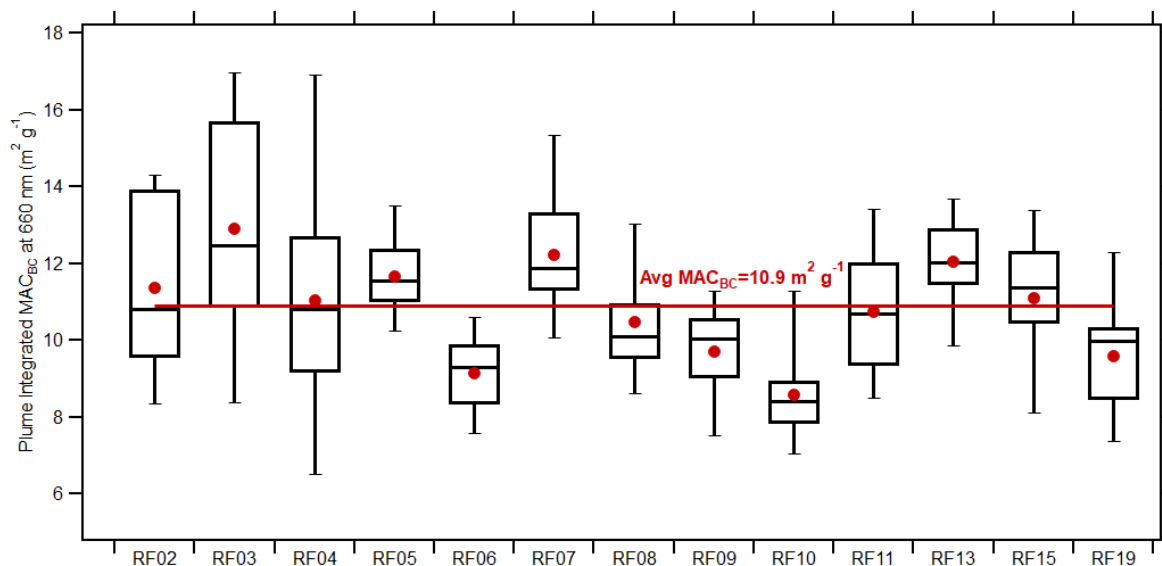


Figure 10: Box plots of plume integrated $\text{MAC}_{\text{BC660}}$ for each flight. On each box the central line represents the median, the top and bottom edges represent the 75th and 25th percentile, and the top and bottom whiskers represent the 90th and 10th percentile of the data. The red dot shows the average, and the red line indicates the average value for all plume integrated $\text{MAC}_{\text{BC660}}$.

594 MAC_{BC660} is also compared with the physical age and MCE (Fig. S13), the O:C and toluene:benzene chemical
595 clocks (Fig. S14), and the altitude, temperature and dilution (ΔCO) (Fig. S15). However, no clear trend is be found in
596 these comparisons.

597 The average absorption enhancement of 1.7 at 660 nm in this study indicates that, on average, 41% of total
598 absorption at 660 nm is caused by lensing and absorbing organics, instead of BC itself. Figure 11 shows the fraction
599 of non-BC absorption from BrC at 660 nm for the biomass burning plumes encountered during WE-CAN using Eq.
600 6-8 with OM calculated from the AMS. The figure is plotted versus plume physical age to allow visualization of the
601 variability, though there is no clear trend with physical age other than perhaps a decrease in variability with increasing
602 physical age. Figure S16 shows a similar result by using OM calculated from the UHSAS. More details on the
603 calculation and the AMS vs. UHSAS methods are explained in section 2.5. Assuming a MAC of the BC core of 6.3
604 $m^2 g^{-1}$, BrC contributes roughly the same amount of absorption at 660 nm as lensing (46% from the AMS method, 62%
605 from the UHSAS method). This means that 19% (AMS method) to 26% (UHSAS method) of the total absorption at
606 660 nm comes from BrC. When different particle density and WSOM:WSOC ratios are considered (top and bottom
607 whiskers, as well as red and blue dashed lines), the fraction of non-BC absorption is 41-49% for the AMS approach
608 (Fig. 11) and 43-80% for the UHSAS approach (Fig. S16) based on different OM:OC and density. The UHSAS
609 approach shows larger uncertainty because it's sensitive to the particle density when calculating particulate mass
610 (Table S1). While there is considerable variability between flights, a rule of thumb that roughly half of the non-BC
611 absorption at red wavelengths is from absorbing organic material seems reasonable. To the best of our knowledge, this
612 is the first observation-based attempt to differentiate between lensing and absorbing organics in the red wavelengths.
613 This approach assumes that water insoluble BrC has the same refractive index as water soluble BrC.

614

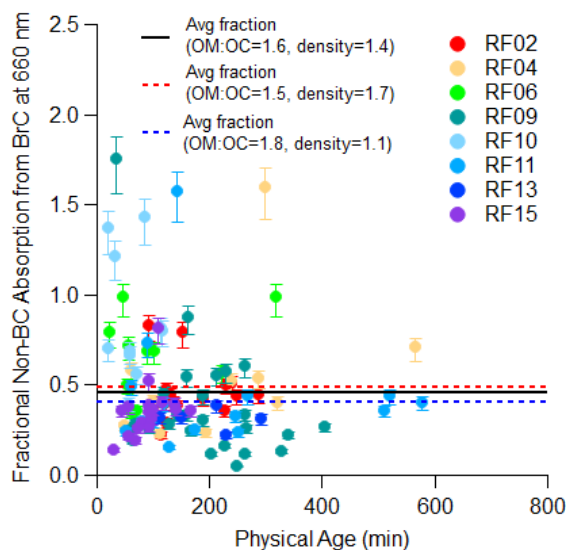


Figure 11: Time evolution of the fraction of non-BC absorption from BrC at 660 nm with AMS and Mie factor. Markers were calculated using a density of 1.4 g cm^{-3} and WSOM:WSOC ratio of 1.6. The top whiskers represent sensitive test values using a density of 1.7 g cm^{-3} and WSOM:WSOC ratio of 1.5, while the bottom whiskers represent sensitive test values using a density of 1.1 g cm^{-3} and WSOM:WSOC ratio of 1.8. The averaged fraction of non-BC absorption from BrC from all the plumes are shown in black solid lines, while the range of this result from sensitivity tests are shown in red and blue dashed lines.

615 4 Conclusion

616 In this study, we presented results that enable a better understanding of the ability of aerosol emissions from
 617 wildfires to absorb visible light and how those properties change after emission. We presented mass absorption
 618 coefficients (MAC) for BC and BrC from Western United States wildfires measured during the WE-CAN campaign
 619 at both short and long visible wavelengths (MAC_{BC660} , $MAC_{BrC+lensing_660}$, MAC_{ws_BrC660} , $MAC_{BrC+lensing_405}$). We also
 620 investigated the bulk absorption coefficient for BrC and bulk scattering coefficient for total aerosol at both short and
 621 long visible wavelengths. General trends that held for all the fire sources are derived, which should be valid throughout
 622 the western U.S. given the wide variety of emissions used to develop them.

623 By utilizing a common parameterization for BrC refractive index from Saleh et al. (2014), with measured
 624 inputs for the BC:OA ratio and particle size, we calculated the theoretical MAC_{BrC660} and MAC_{BrC405} , and they were
 625 2.3~3.4 times larger than the measured $MAC_{BrC+lensing}$ during WE-CAN. While this discrepancy has been resolved
 626 previously by implementing bleaching into model schemes, we show that this is probably the incorrect explanation
 627 given the MAC of BrC either remains constant or slightly increases when chemical markers (O:C, toluene:benzene)
 628 suggest more oxidation has occurred. We suggest a different parameterization of the refractive index is needed to
 629 represent wildfire optical properties in the Western United States rather than using bleaching to decrease the mass
 630 absorption cross section (MAC) of the Saleh parameterization. We also note that there needs to be better terminology
 631 to distinguish between decreasing absorption caused by losses of organic aerosol mass versus decreasing absorption
 632 caused by changes in the MAC of the aerosol.

633 In the blue visible wavelengths, where BrC is more often thought about, $MAC_{BrC+lensing_405}$ is $0.59 \pm 0.19 \text{ m}^2$
634 g^{-1} and shows little variation with physical age, MCE, altitude, temperature or BC:OA ratio. There isn't any decreasing
635 trends in all the MAC_{BrC} data we obtained (MAC_{ws_BrC405} , $MAC_{BrC+lensing_405}$, MAC_{ws_BrC660} , and $MAC_{BrC+lensing_660}$)
636 with markers of chemical age (toluene:benzene, O:C), but bulk absorption of BrC does decrease with these same
637 markers. In highly aged plumes from multiple fires (RF05 and RF08), the $MAC_{BrC+lensing_405}$ has an average value of
638 $0.63 \pm 0.2 \text{ m}^2 \text{ g}^{-1}$, suggesting that brown carbon remains significantly absorbing even at relatively longer ages.

639 We find that total organic aerosol (OA) and water-soluble organic carbon (WSOC) are strongly correlated
640 with chemical markers of oxidative age. OA and WSOC (both normalized to CO) decrease with decreasing
641 toluene:benzene ratio and increasing O:C ratio. However, this phenomenon is only clearly observed when data from
642 all the observed fires is included rather than during the aging of individual fire plumes. This could mean that the fires
643 either had different emission ratios of toluene:benzene and O:C or the smoke underwent rapid secondary chemistry
644 prior to the first plume pass in WE-CAN. Regardless, the correlations are fairly robust (R^2 of 0.4 to 0.8) given the
645 many variables (MCE, fuel type, etc.) that are changing in the dataset and provide a potential link between chemical
646 markers and total organic aerosol amounts across a wide range of fires. While OA and WSOC decrease with decreasing
647 toluene:benzene or increasing O:C, MAC_{BrC} actually shows a weak increasing trend with these same markers of aging,
648 showing that while the total amount of organic aerosol is decreasing, the ability of the organic to absorb per mass is
649 staying relatively constant, or even increasing. We also found that the bulk scattering coefficient (normalized to CO)
650 decreases with decreasing toluene:benzene ratio or increasing O:C ratio due to less OA being present, which leads to
651 a very different net radiative effect than that which results from just changing the refractive index of BrC.

652 In the red visible wavelengths, where BrC is often less noticed, we observed that the MAC of BC stayed
653 relatively constant across all plumes measured and at all physical ages (ages up to 15 hours observed), with an averaged
654 MAC_{BC660} of $10.9 \pm 2.1 \text{ m}^2 \text{ g}^{-1}$ (average \pm standard deviation), which includes the contribution from both lensing effect
655 and absorbing organics. This average showed no clear trends with altitude or temperature, and we saw no evidence
656 that MAC_{BC660} is correlated to MCE. Even in highly aged plumes with emissions mixed from multiple fires (RF05
657 and RF08), the MAC_{BC660} is similar in magnitude to the near-source plumes with an average of $11.3 \pm 1.8 \text{ m}^2 \text{ g}^{-1}$. Both
658 the fact that this MAC is significantly larger than the MAC for uncoated BC (often cited to be $\sim 6.3 \text{ m}^2 \text{ g}^{-1}$) and the
659 fact that the MAC remains relatively constant across different fires and different plume ages are key insights that can
660 improve models of aerosol optical properties in wildfire emissions.

661 Through a novel use of PILS data, we find that BrC contributes 41-80% of non-BC absorption at 660 nm
662 (assuming $6.3 \text{ m}^2 \text{ g}^{-1}$ as the MAC of BC core at 660 nm). BrC contributes, on average, 26% of total absorption, but
663 the absorption cross section of water-soluble BrC is relatively small at 660 nm, with a MAC_{ws_BrC660} of $0.03 \pm 0.02 \text{ m}^2$
664 g^{-1} , which does not change with physical age, and no trend with MCE is observed. The average $MAC_{BrC+lensing_660}$
665 derived from the PAS (which includes both brown carbon absorption and lensing of black carbon) is $0.11 \pm 0.06 \text{ m}^2$
666 g^{-1} .

667 **Data Availability**

668 The WE-CAN data can be found at http://data.eol.ucar.edu/master_lists/generated/we-can/.

669 The DOI for each data set used in this work are:
670 PAS and CAPS PM_{SSA}: <https://doi.org/10.26023/K8P0-X4T3-TN06>
671 PILS1: <https://doi.org/10.26023/9H07-MD9K-430D> and <https://doi.org/10.26023/CRHY-NDT9-C30V>
672 PILS2: <https://doi.org/10.26023/7TAN-TZMD-680Y>
673 SP2: <https://doi.org/10.26023/P8R2-RAB6-N814>
674 UHSAS: <https://doi.org/10.26023/BZ4F-EAC4-290W>
675 PTR-ToF-MS: <https://doi.org/10.26023/K9F4-2CNH-EQ0W>
676 HR-AMS: <https://doi.org/10.26023/MM2Y-ZGFQ-RB0B>
677 Picarro: <https://doi.org/10.26023/NNYM-Z18J-PX0Q>
678 miniQCL: <https://doi.org/10.26023/Q888-WZRD-B70F>

679 **Author Contributions**

680 SMM designed the project. YS wrote the paper. YS, RPP, APS, EJTL, LAG, DKF, WP, LH, DWT, TC, EVF, and SMM
681 collected and analyzed data.

682 **Competing Interests**

683 The authors declare that they have no conflict of interest.

684 **Acknowledgements**

685 The 2018 WE-CAN field campaign was supported by the U.S. National Science Foundation through grants AGS-
686 1650493 (U of Wyoming), AGS-1650786 (Colorado State U), AGS-1650275 (U of Montana), AGS-1650288 (U of
687 Colorado at Boulder), and the National Oceanic and Atmospheric Administration (Award # NA17OAR4310010,
688 Colorado State U). This material is based upon study supported by the National Center for Atmospheric Research,
689 which is a major facility sponsored by the National Science Foundation under Cooperative Agreement no. 1852977.
690 The authors acknowledge support from AGS-1650493 for YS, SMM and RPP, AGS-1650786 for APS and EJTL,
691 AGS-2144896 for LH and WP, AGS-1650288 for DWT, NOAA Climate Program Office's Atmospheric Chemistry,
692 Carbon Cycle, and Climate program (Grant NA17OAR4310010) for DKF and LAG.

693

694 We sincerely thank Ernie Lewis for his work implementing Mie theory into Igor code.

695 **References**

696 Aiken, A. C., Decarlo, P. F., Kroll, J. H., Worsnop, D. R., Huffman, J. A., Docherty, K. S., Ulbrich, I. M., Mohr, C.,
697 Kimmel, J. R., Sueper, D., Sun, Y., Zhang, Q., Trimborn, A., Northway, M., Ziemann, P. J., Canagaratna, M. R.,
698 Onasch, T. B., Alfarra, M. R., Prevot, A. S. H., Dommen, J., Duplissy, J., Metzger, A., Baltensperger, U. and

699 Jimenez, J. L.: O/C and OM/OC ratios of primary, secondary, and ambient organic aerosols with high-resolution
700 time-of-flight aerosol mass spectrometry, *Environ. Sci. Technol.*, 42(12), 4478–4485, doi:10.1021/es703009q,
701 2008.

702 Akagi, S. K., Yokelson, R. J., Wiedinmyer, C., Alvarado, M. J., Reid, J. S., Karl, T., Crounse, J. D. and Wennberg, P.
703 O.: Emission factors for open and domestic biomass burning for use in atmospheric models, *Atmos. Chem. Phys.*,
704 11(9), 4039–4072, doi:10.5194/acp-11-4039-2011, 2011.

705 Andreae, M. O.: Emission of trace gases and aerosols from biomass burning – An updated assessment, *Atmos. Chem.*
706 *Phys. Discuss.*, 1–27, doi:10.5194/acp-2019-303, 2019.

707 Andreae, M. O. and Gelencsér, A.: Black carbon or brown carbon? The nature of light-absorbing carbonaceous
708 aerosols, *Atmos. Chem. Phys.*, 6, 3131–3148, doi:10.5194/acp-6-3131-2006, 2006.

709 Bahadur, R., Praveen, P. S., Xu, Y. and Ramanathan, V.: Solar absorption by elemental and brown carbon determined
710 from spectral observations, *Proc. Natl. Acad. Sci.*, 109(43), 17366–17371, doi:10.1073/pnas.1205910109, 2012.

711 Bohren, C. F. and Huffman, D. R.: *Absorption and scattering of light by small particles.*, 1983.

712 Bond, T. C. and Bergstrom, R. W.: Light absorption by carbonaceous particles: An investigative review, *Aerosol Sci.*
713 *Technol.*, 40(1), 27–67, doi:10.1080/02786820500421521, 2006.

714 Bond, T. C., Habib, G. and Bergstrom, R. W.: Limitations in the enhancement of visible light absorption due to mixing
715 state, *J. Geophys. Res. Atmos.*, 111(20), 1–13, doi:10.1029/2006JD007315, 2006.

716 Bond, T. C., Doherty, S. J., Fahey, D. W., Forster, P. M., Berntsen, T., Deangelo, B. J., Flanner, M. G., Ghan, S.,
717 Kärcher, B., Koch, D., Kinne, S., Kondo, Y., Quinn, P. K., Sarofim, M. C., Schultz, M. G., Schulz, M.,
718 Venkataraman, C., Zhang, H., Zhang, S., Bellouin, N., Guttikunda, S. K., Hopke, P. K., Jacobson, M. Z., Kaiser, J.
719 W., Klimont, Z., Lohmann, U., Schwarz, J. P., Shindell, D., Storelvmo, T., Warren, S. G. and Zender, C. S.:
720 Bounding the role of black carbon in the climate system: A scientific assessment, *J. Geophys. Res. Atmos.*, 118(11),
721 5380–5552, doi:10.1002/jgrd.50171, 2013.

722 Brown, H., Liu, X., Feng, Y., Jiang, Y., Wu, M., Lu, Z., Wu, C., Murphy, S. and Pokhrel, R.: Radiative effect and
723 climate impacts of brown carbon with the Community Atmosphere Model (CAM5), *Atmos. Chem. Phys.*, 18(24),
724 17745–17768, doi:10.5194/acp-18-17745-2018, 2018.

725 Brown, H., Liu, X., Pokhrel, R., Murphy, S., Lu, Z., Saleh, R., Mielonen, T., Kokkola, H., Bergman, T., Myhre, G.,
726 Skeie, R. B., Watson-Paris, D., Stier, P., Johnson, B., Bellouin, N., Schulz, M., Vakkari, V., Beukes, J. P., van Zyl,
727 P. G., Liu, S. and Chand, D.: Biomass burning aerosols in most climate models are too absorbing, *Nat. Commun.*,
728 12(1), 1–15, doi:10.1038/s41467-020-20482-9, 2021.

729 Burke, M., Driscoll, A., Heft-Neal, S., Xue, J., Burney, J. and Wara, M.: The changing risk and burden of wildfire in
730 the United States, *Proc. Natl. Acad. Sci. U. S. A.*, 118(2), 1–6, doi:10.1073/PNAS.2011048118, 2021.

731 Canagaratna, M. R., Jimenez, J. L., Kroll, J. H., Chen, Q., Kessler, S. H., Massoli, P., Hildebrandt Ruiz, L., Fortner,
732 E., Williams, L. R., Wilson, K. R., Surratt, J. D., Donahue, N. M., Jayne, J. T. and Worsnop, D. R.: Elemental ratio
733 measurements of organic compounds using aerosol mass spectrometry : characterization , improved calibration ,
734 and implications, *Atmos. Chem. Phys.*, 15(1), 253–272, doi:10.5194/acp-15-253-2015, 2015.

735 Cappa, C. D., Onasch, T. B., Massoli, P., Worsnop, D. R., Bates, T. S., Cross, E. S., Davidovits, P., Hakala, J., Hayden,
736 K. L., Jobson, B. T., Kolesar, K. R., Lack, D. A., Lerner, B. M., Li, S. M., Mellon, D., Nuaaman, I., Olfert, J. S.,
737 Petäjä, T., Quinn, P. K., Song, C., Subramanian, R., Williams, E. J. and Zaveri, R. A.: Radiative absorption
738 enhancements due to the mixing state of atmospheric black carbon, *Science* (80-.), 337(6098), 1078–1081,
739 doi:10.1126/science.1223447, 2012.

740 Cappa, C. D., Zhang, X., Russell, L. M., Collier, S., Lee, A. K. Y., Chen, C. L., Betha, R., Chen, S., Liu, J., Price, D.
741 J., Sanchez, K. J., McMeeking, G. R., Williams, L. R., Onasch, T. B., Worsnop, D. R., Abbatt, J. and Zhang, Q.:
742 Light Absorption by Ambient Black and Brown Carbon and its Dependence on Black Carbon Coating State for
743 Two California, USA, Cities in Winter and Summer, *J. Geophys. Res. Atmos.*, 124(3), 1550–1577,
744 doi:10.1029/2018JD029501, 2019.

745 Carter, T. S., Heald, C. L., Cappa, C. D., Kroll, J. H., Campos, T. L., Coe, H., Cotterell, M. I., Davies, N. W., Farmer,
746 D. K., Fox, C., Garofalo, L. A., Hu, L., Langridge, J. M., Levin, E. J. T., Murphy, S., Pokhrel, R., Shen, Y., Szpek,
747 K., Taylor, J. W. and Wu, H.: Investigating Carbonaceous Aerosol and its Absorption Properties from Fires in the
748 western US (WE-CAN) and southern Africa (ORACLES and CLARIFY), *J. Geophys. Res. Atmos.*, 1–28,
749 doi:10.1029/2021JD034984, 2021.

750 Chen, M., Sun, Z., Davis, J. M., Liu, Y. A., Corr, C. A. and Gao, W.: Improving the mean and uncertainty of ultraviolet
751 multi-filter rotating shadowband radiometer in situ calibration factors: Utilizing Gaussian process regression with
752 a new method to estimate dynamic input uncertainty, *Atmos. Meas. Tech.*, 12(2), 935–953, doi:10.5194/amt-12-
753 935-2019, 2019.

754 Cho, C., Kim, S. W., Lee, M., Lim, S., Fang, W., Gustafsson, Ö., Andersson, A., Park, R. J. and Sheridan, P. J.:
755 Observation-based estimates of the mass absorption cross-section of black and brown carbon and their contribution
756 to aerosol light absorption in East Asia, *Atmos. Environ.*, 212(November 2018), 65–74,
757 doi:10.1016/j.atmosenv.2019.05.024, 2019.

758 Craig, L., Moharreri, A., Schanot, A., Rogers, D. C., Dhaniyala, S., Craig, L., Anderson, B. and Dhaniyala, S.:
759 Characterizations of Cloud Droplet Shatter Artifacts in Two Airborne Aerosol Inlets, *Aerosol Sci. Technol.*, 47:6,
760 662–671, doi:10.1080/02786826.2013.780648, 2013a.

761 Craig, L., Schanot, A., Moharreri, A., Rogers, D. C. and Dhaniyala, S.: Design and Sampling Characteristics of a New
762 Airborne Aerosol Inlet for Aerosol Measurements in Clouds, *J. Atmos. Ocean. Technol.*, 30, 1123–1135,
763 doi:10.1175/JTECH-D-12-00168.1, 2013b.

764 Duarte, R. M. B. O., Freire, S. M. S. C. and Duarte, A. C.: Investigating the water-soluble organic functionality of
765 urban aerosols using two-dimensional correlation of solid-state ¹³C NMR and FTIR spectral data, *Atmos. Environ.*,
766 116, 245–252, doi:10.1016/j.atmosenv.2015.06.043, 2015.

767 Duarte, R. M. B. O., Piñeiro-Iglesias, M., López-Mahía, P., Muniategui-Lorenzo, S., Moreda-Piñeiro, J., Silva, A. M.
768 S. and Duarte, A. C.: Comparative study of atmospheric water-soluble organic aerosols composition in contrasting
769 suburban environments in the Iberian Peninsula Coast, *Sci. Total Environ.*, 648, 430–441,
770 doi:10.1016/j.scitotenv.2018.08.171, 2019.

771 Eatough, D. J., Wadsworth, A., Eatough, D. A., Crawford, J. W., Hansen, L. D. and Lewis, E. A.: A multiple-system,
772 multi-channel diffusion denuder sampler for the determination of fine-particulate organic material in the
773 atmosphere, *Atmos. Environ. Part A, Gen. Top.*, 27(8), 1213–1219, doi:10.1016/0960-1686(93)90247-V, 1993.

774 Finessi, E., Decesari, S., Paglione, M., Giulianelli, L., Carbone, C., Gilardoni, S., Fuzzi, S., Saarikoski, S., Raatikainen,
775 T., Hillamo, R., Allan, J., Mentel, T. F., Tiitta, P., Laaksonen, A., Petäjä, T., Kulmala, M., Worsnop, D. R. and
776 Facchini, M. C.: Determination of the biogenic secondary organic aerosol fraction in the boreal forest by NMR
777 spectroscopy, *Atmos. Chem. Phys.*, 12(2), 941–959, doi:10.5194/acp-12-941-2012, 2012.

778 Ford, B., Val Martin, M., Zelasky, S. E., Fischer, E. V., Anenberg, S. C., Heald, C. L. and Pierce, J. R.: Future Fire
779 Impacts on Smoke Concentrations, Visibility, and Health in the Contiguous United States, *GeoHealth*, 2(8), 229–
780 247, doi:10.1029/2018gh000144, 2018.

781 Forrister, Haviland; Liu, Jiumeng; Scheuer, Eric; Dibb, Jack; Ziemba, Luke; Thornhill, L. Kenneth; Anderson, Bruce;
782 Diskin, Glenn; Perring, E. Anne; P. Schwarz, Joshua; Campuzano-Jost, Pedro; A. Day, Douglas; B. Palm, Brett;
783 Jimenez, L. Jose; Nenes, Athan, R. J.: Evolution of brown carbon in wildfire plumes, *Geophys. Res. Lett.*, 42,
784 4623–4630, doi:10.1002/2015GL063897, 2015.

785 Foster, K., Pokhrel, R., Burkhart, M. and Murphy, S.: A novel approach to calibrating a photoacoustic absorption
786 spectrometer using polydisperse absorbing aerosol, *Atmos. Meas. Tech.*, 12(6), 3351–3363, doi:10.5194/amt-12-
787 3351-2019, 2019.

788 Fuller, K. A. and Kreidenweis, S. M.: Effects of mixing on extinction by carbonaceous particles, *J. Geophys. Res.*,
789 104(D13), 15941–15954, doi:10.1029/1998JD100069, 1999.

790 Garofalo, L. A., Pothier, M. A., Levin, E. J. T., Campos, T., Kreidenweis, S. M. and Farmer, D. K.: Emission and
791 Evolution of Submicron Organic Aerosol in Smoke from Wildfires in the Western United States, *ACS Earth Sp.*
792 *Chem.*, 3(7), 1237–1247, doi:10.1021/acsearthspacechem.9b00125, 2019.

793 Gouw, J. A. De, Middlebrook, A. M., Warneke, C., Goldan, P. D., Kuster, W. C., Roberts, J. M., Fehsenfeld, F. C.,
794 Worsnop, D. R., Canagaratna, M. R., Pszenny, A. A. P., Keene, W. C., Marchewka, M., Bertman, S. B. and Bates,
795 T. S.: Budget of organic carbon in a polluted atmosphere : Results from the New England Air Quality Study in
796 2002, *J. Geophys. Res.*, 110, 1–22, doi:10.1029/2004JD005623, 2005.

797 Grieshop, A. P., Logue, J. M., Donahue, N. M. and Robinson, A. L.: Laboratory investigation of photochemical
798 oxidation of organic aerosol from wood fires 1: Measurement and simulation of organic aerosol evolution, *Atmos.*
799 *Chem. Phys.*, 9(4), 1263–1277, doi:10.5194/acp-9-1263-2009, 2009.

800 Healy, R. M., Wang, J. M., Jeong, C. H., Lee, A. K. Y., Willis, M. D., Jaroudi, E., Zimmerman, N., Hilker, N., Murphy,
801 M., Eckhardt, S., Stohl, A., Abbatt, J. P. D., Wenger, J. C. and Evans, G. J.: Light-absorbing properties of ambient
802 black carbon and brown carbon from fossil fuel and biomass burning sources, *J. Geophys. Res. Atmos.*, 120(13),
803 6619–6633, doi:10.1002/2015JD023382, 2015.

804 Hecobian, A., Zhang, X., Zheng, M., Frank, N., Edgerton, E. S. and Weber, R. J.: Water-soluble organic aerosol
805 material and the light-absorption characteristics of aqueous extracts measured over the Southeastern United States,
806 *Atmos. Chem. Phys.*, 10(13), 5965–5977, doi:10.5194/acp-10-5965-2010, 2010.

807 Hurteau, M. D., Westerling, A. L., Wiedinmyer, C. and Bryant, B. P.: Projected effects of climate and development on
808 California wildfire emissions through 2100, *Environ. Sci. Technol.*, 48(4), 2298–2304, doi:10.1021/es4050133,
809 2014.

810 Kelesidis, G. A., Neubauer, D., Fan, L. S., Lohmann, U. and Pratsinis, S. E.: Enhanced Light Absorption and Radiative
811 Forcing by Black Carbon Agglomerates, *Environ. Sci. Technol.*, 56(12), 8610–8618, doi:10.1021/acs.est.2c00428,
812 2022.

813 Kirchstetter, T. W., Novakov, T. and Hobbs, P. V.: Evidence that the spectral dependence of light absorption by aerosols
814 is affected by organic carbon, *J. Geophys. Res. D Atmos.*, 109(21), 1–12, doi:10.1029/2004JD004999, 2004.

815 Krasowsky, T. S., McMeeking, G. R., Wang, D., Sioutas, C. and Ban-Weiss, G. A.: Measurements of the impact of
816 atmospheric aging on physical and optical properties of ambient black carbon particles in Los Angeles, *Atmos.*
817 *Environ.*, 142, 496–504, doi:10.1016/j.atmosenv.2016.08.010, 2016.

818 Lack, D. A., Lovejoy, E. R., Baynard, T., Pettersson, A. and Ravishankara, A. R.: Aerosol Absorption Measurement
819 using Photoacoustic Spectroscopy: Sensitivity, Calibration, and Uncertainty Developments, *Aerosol Sci. Technol.*,
820 40(9), 697–708, doi:10.1080/02786820600803917, 2006.

821 Lack, D. A. and Cappa, C. D.: Impact of brown and clear carbon on light absorption enhancement, single scatter
822 albedo and absorption wavelength dependence of black carbon, *Atmos. Chem. Phys.*, 10(9), 4207–4220,
823 doi:10.5194/acp-10-4207-2010, 2010.

824 Lack, D. A., Langridge, J. M., Bahreini, R., Cappa, C. D., Middlebrook, A. M. and Schwarz, J. P.: Brown carbon and
825 internal mixing in biomass burning particles, *Proc. Natl. Acad. Sci. U. S. A.*, 109(37), 14802–14807,
826 doi:10.1073/pnas.1206575109, 2012a.

827 Lack, D. A., Richardson, M. S., Law, D., Langridge, J. M., Cappa, C. D., McLaughlin, R. J. and Murphy, D. M.:
828 Aircraft Instrument for Comprehensive Characterization of Aerosol Optical Properties, Part 2: Black and Brown
829 Carbon Absorption and Absorption Enhancement Measured with Photo Acoustic Spectroscopy, *Aerosol Sci.*
830 *Technol.*, 46(5), 555–568, doi:10.1080/02786826.2011.645955, 2012b.

831 Lindaas, J., Pollack, I. B., Garofalo, L. A., Pothier, M. A., Farmer, D. K., Kreidenweis, S. M., Campos, T. L., Flocke,
832 F., Weinheimer, A. J., Montzka, D. D., Tyndall, G. S., Palm, B. B., Peng, Q., Thornton, J. A., Permar, W., Wielgasz,
833 C., Hu, L., Ottmar, R. D., Restaino, J. C., Hudak, A. T., Ku, I. T., Zhou, Y., Sive, B. C., Sullivan, A., Collett, J. L.
834 and Fischer, E. V.: Emissions of Reactive Nitrogen From Western U.S. Wildfires During Summer 2018, *J. Geophys.*
835 *Res. Atmos.*, 126(2), 1–21, doi:10.1029/2020JD032657, 2021.

836 Liu, D., Whitehead, J., Alfara, M. R., Reyes-villegas, E., Spracklen, D. V, Reddington, C. L., Kong, S., Williams, P.
837 I., Ting, Y., Haslett, S., Taylor, J. W., Flynn, M. J., Morgan, W. T., Mcfiggans, G., Coe, H. and Allan, J. D.: Black-
838 carbon absorption enhancement in the atmosphere determined by particle mixing state, *Nat. Geosci.*, 10(3), 184–
839 188, doi:10.1038/NGEO2901, 2017.

840 Liu, D., He, C., Schwarz, J. P. and Wang, X.: Lifecycle of light-absorbing carbonaceous aerosols in the atmosphere,
841 *npj Clim. Atmos. Sci.*, 3(40), doi:10.1038/s41612-020-00145-8, 2020.

842 Liu, J., Bergin, M., Guo, H., King, L., Kotra, N., Edgerton, E. and Weber, R. J.: Size-resolved measurements of brown
843 carbon in water and methanol extracts and estimates of their contribution to ambient fine-particle light absorption,
844 *Atmos. Chem. Phys.*, 13(24), 12389–12404, doi:10.5194/acp-13-12389-2013, 2013.

845 Liu, S., Aiken, A. C., Gorkowski, K., Dubey, M. K., Cappa, C. D., Williams, L. R., Herndon, S. C., Massoli, P., Fortner,
846 E. C., Chhabra, P. S., Brooks, W. A., Onasch, T. B., Jayne, J. T., Worsnop, D. R., China, S., Sharma, N., Mazzoleni,
847 C., Xu, L., Ng, N. L., Liu, D., Allan, J. D., Lee, J. D., Fleming, Z. L., Mohr, C., Zotter, P., Szidat, S. and Prévôt,
848 A. S. H.: Enhanced light absorption by mixed source black and brown carbon particles in UK winter, *Nat.*
849 *Commun.*, 6, 8435, doi:10.1038/ncomms9435, 2015.

850 Marple, V. A., Rubow, K. L. and Behm, S. M.: A microorifice uniform deposit impactor (moudi): Description,
851 calibration, and use, *Aerosol Sci. Technol.*, 14(4), 434–436, doi:10.1080/02786829108959504, 1991.

852 McClure, C. D., Lim, C. Y., Hagan, D. H., Kroll, J. H. and Cappa, C. D.: Biomass-burning-derived particles from a
853 wide variety of fuels - Part 1: Properties of primary particles, *Atmos. Chem. Phys.*, 20(3), 1531–1547,
854 doi:10.5194/acp-20-1531-2020, 2020.

855 McConnell, J. R., Edwards, R., Kok, L. G., Flanner, M. G., Zender, C. S., Saltzman, E. S., Banta, J. R., Pasteris, D.
856 R., Carter, M. M. and Kahl, J. D. W.: 20th-Century Industrial Black Carbon Emissions Altered Arctic Climate
857 Forcing, *Science* (80-.), 317(5843), 1381–1384, doi:10.1126/science.1144856, 2007.

858 Moharreri, A., Craig, L., Dubey, P., Rogers, D. C. and Dhaniyala, S.: Aircraft testing of the new Blunt-body Aerosol
859 Sampler (BASE), *Atmos. Meas. Tech.*, 7(9), 3085–3093, doi:10.5194/amt-7-3085-2014, 2014.

860 Neumann, J. E., Amend, M., Anenberg, S., Kinney, P. L., Sarofim, M., Martinich, J., Lukens, J., Xu, J. W. and Roman,
861 H.: Estimating PM_{2.5}-related premature mortality and morbidity associated with future wildfire emissions in the
862 western US, *Environ. Res. Lett.*, 16(3), doi:10.1088/1748-9326/abe82b, 2021.

863 Onasch, T. B., Massoli, P., Kebejian, P. L., Hills, F. B., Bacon, F. W. and Freedman, A.: Single scattering albedo
864 monitor for airborne particulates, *Aerosol Sci. Technol.*, 49(4), 267–279, doi:10.1080/02786826.2015.1022248,
865 2015.

866 Orsini, D. A., Ma, Y., Sullivan, A., Sierau, B., Baumann, K. and Weber, R. J.: Refinements to the particle-into-liquid
867 sampler (PILS) for ground and airborne measurements of water soluble aerosol composition, *Atmos. Environ.*,
868 37(9–10), 1243–1259, doi:10.1016/S1352-2310(02)01015-4, 2003.

869 Palm, B. B., Peng, Q., Fredrickson, C. D., Lee, B. H., Garofalo, L. A., Pothier, M. A., Kreidenweis, S. M., Farmer, D.
870 K., Pokhrel, R. P., Shen, Y., Murphy, S. M., Permar, W., Hu, L., Campos, T. L., Hall, S. R., Ullmann, K., Zhang,
871 X., Flocke, F., Fischer, E. V. and Thornton, J. A.: Quantification of organic aerosol and brown carbon evolution in
872 fresh wildfire plumes, *Proc. Natl. Acad. Sci. U. S. A.*, 117(47), 29469–29477, doi:10.1073/pnas.2012218117, 2020.

873 Peltier, R. E., Weber, R. J. and Sullivan, A. P.: Investigating a liquid-based method for online organic carbon detection
874 in atmospheric particles, *Aerosol Sci. Technol.*, 41(12), 1117–1127, doi:10.1080/02786820701777465, 2007.

875 Peng, J., Hu, M., Guo, S., Du, Z., Zheng, J., Shang, D., Zamora, M. L., Zeng, L., Shao, M., Wu, Y. S., Zheng, J., Wang,
876 Y., Glen, C. R., Collins, D. R., Molina, M. J. and Zhang, R.: Markedly enhanced absorption and direct radiative
877 forcing of black carbon under polluted urban environments, *Proc. Natl. Acad. Sci. U. S. A.*, 113(16), 4266–4271,
878 doi:10.1073/pnas.1602310113, 2016.

879 Permar, W., Wang, Q., Selimovic, V., Wielgasz, C., Yokelson, R. J., Hornbrook, R. S., Hills, A. J., Apel, E. C., Ku, I.
880 T., Zhou, Y., Sive, B. C., Sullivan, A. P., Collett, J. L., Campos, T. L., Palm, B. B., Peng, Q., Thornton, J. A.,
881 Garofalo, L. A., Farmer, D. K., Kreidenweis, S. M., Levin, E. J. T., DeMott, P. J., Flocke, F., Fischer, E. V. and Hu,
882 L.: Emissions of Trace Organic Gases From Western U.S. Wildfires Based on WE-CAN Aircraft Measurements,
883 *J. Geophys. Res. Atmos.*, 126(11), doi:10.1029/2020JD033838, 2021.

884 Pokhrel, R. P., Wagner, N. L., Langridge, J. M., Lack, D. A., Jayarathne, T., Stone, E. A., Stockwell, C. E., Yokelson,
885 R. J. and Murphy, S. M.: Parameterization of single-scattering albedo (SSA) and absorption Ångström exponent
886 (AAE) with EC/OC for aerosol emissions from biomass burning, *Atmos. Chem. Phys.*, 16(15), 9549–9561,
887 doi:10.5194/acp-16-9549-2016, 2016.

888 Pokhrel, R. P., Beamesderfer, E. R., Wagner, N. L., Langridge, J. M., Lack, D. A., Jayarathne, T., Stone, E. A.,
889 Stockwell, C. E., Yokelson, R. J. and Murphy, S. M.: Relative importance of black carbon, brown carbon, and
890 absorption enhancement from clear coatings in biomass burning emissions, *Atmos. Chem. Phys.*, 17(8), 5063–
891 5078, doi:10.5194/acp-17-5063-2017, 2017.

892 Romshoo, B., Müller, T., Pfeifer, S., Saturno, J., Nowak, A., Ciupek, K., Quincey, P. and Wiedensohler, A.: Optical
893 properties of coated black carbon aggregates: Numerical simulations, radiative forcing estimates, and size-resolved
894 parameterization scheme, *Atmos. Chem. Phys.*, 21(17), 12989–13010, doi:10.5194/acp-21-12989-2021, 2021.

895 Rosencwaig, A.: Photoacoustic spectroscopy., *Annu. Rev. Biophys. Bioeng.*, 9, 31–54,
896 doi:10.1146/annurev.bb.09.060180.000335, 1980.

897 Saleh, R., Robinson, E. S., Tkacik, D. S., Ahern, A. T., Liu, S., Aiken, A. C., Sullivan, R. C., Presto, A. A., Dubey, M.
898 K., Yokelson, R. J., Donahue, N. M. and Robinson, A. L.: Brownness of organics in aerosols from biomass burning
899 linked to their black carbon content, *Nat. Geosci.*, 7(9), 647–650, doi:10.1038/ngeo2220, 2014.

900 Saleh, R.: From Measurements to Models: Toward Accurate Representation of Brown Carbon in Climate Calculations,
901 *Curr. Pollut. Reports*, 6(2), 90–104, doi:10.1007/s40726-020-00139-3, 2020.

902 Sarangi, C., Qian, Y., Rittger, K., Leung, R. L., Chand, D., Bormann, K. J. and Painter, T. H.: Dust dominates high-
903 altitude snow darkening and melt over high-mountain Asia, *Nat. Clim. Chang.*, (October), 1–7,
904 doi:10.1038/s41558-020-00909-3, 2020.

905 Schnaiter, M., Horvath, H., Möhler, O., Naumann, K. H., Saathoff, H. and Schöck, O. W.: UV-VIS-NIR spectral optical
906 properties of soot and soot-containing aerosols, *J. Aerosol Sci.*, 34(10), 1421–1444, doi:10.1016/S0021-
907 8502(03)00361-6, 2003.

908 Schnaiter, M., Linke, C., Möhler, O., Naumann, K. H., Saathoff, H., Wagner, R., Schurath, U. and Wehner, B.:
909 Absorption amplification of black carbon internally mixed with secondary organic aerosol, *J. Geophys. Res. D*
910 *Atmos.*, 110(19), 1–11, doi:10.1029/2005JD006046, 2005.

911 Schwarz, J. P., Gao, R. S., Fahey, D. W., Thomson, D. S., Watts, L. A., Wilson, J. C., Reeves, J. M., Darbeheshti, M.,
912 Baumgardner, D. G., Kok, G. L., Chung, S. H., Schulz, M., Hendricks, J., Lauer, A., Ka, B., Slowik, J. G., Rosenlof,
913 K. H., Thompson, T. L., Langford, A. O., Loewenstein, M. and Aikin, K. C.: Single-particle measurements of
914 midlatitude black carbon and light-scattering aerosols from the boundary layer to the lower stratosphere, *J.*
915 *Geophys. Res.*, 111, D16207, doi:10.1029/2006JD007076, 2006.

916 Subramanian, R., Kok, G. L., Baumgardner, D., Clarke, A., Shinozuka, Y., Campos, T. L., Heizer, C. G., Stephens, B.
917 B., De Foy, B., Voss, P. B. and Zaveri, R. A.: Black carbon over Mexico: The effect of atmospheric transport on
918 mixing state, mass absorption cross-section, and BC/CO ratios, *Atmos. Chem. Phys.*, 10(1), 219–237,
919 doi:10.5194/acp-10-219-2010, 2010.

920 Sullivan, A. P., Pokhrel, R. P., Shen, Y., Murphy, S. M., Toohey, D. W., Campos, T., Lindaas, J., Fischer, E. V. and
921 Collett, J. L.: Examination of Brown Carbon Absorption from Wildfires in the Western U.S. During the WE-CAN
922 Study, *Atmos. Chem. Phys. Discuss.*, (July), 1–29, doi:10.5194/acp-2022-459, 2022.

923 Sun, Y., Zhang, Q., Zheng, M., Ding, X., Edgerton, E. S. and Wang, X.: Characterization and source apportionment
924 of water-soluble organic matter in atmospheric fine particles (PM_{2.5}) with high-resolution aerosol mass
925 spectrometry and GC-MS, *Environ. Sci. Technol.*, 45(11), 4854–4861, doi:10.1021/es200162h, 2011.

926 Szopa, S., V. Naik, B. Adhikary, P. Artaxo, T. Berntsen, W.D. Collins, S. Fuzzi, L. Gallardo, A. Kiendler-Scharr, Z.
927 Klimont, H. Liao, N. Unger, and P. Zanis: Short-Lived Climate Forcers. In *Climate Change 2021: The Physical
928 Science Basis. Contribution of Working Group I to the Sixth Assessment Report of the Intergovernmental Panel
929 on Climate Change*. Cambridge University Press, Cambridge, United Kingdom and New York, NY, USA, pp. 817–
930 922, doi:10.1017/9781009157896.008, 2021.

931 Tasoglou, A., Louvaris, E., Florou, K., Liangou, A., Karnezi, E., Kaltsonoudis, C., Wang, N. and Pandis, S. N.: Aerosol
932 light absorption and the role of extremely low volatility organic compounds, *Atmos. Chem. Phys.*, 20(19), 11625–
933 11637, doi:10.5194/acp-20-11625-2020, 2020.

934 Taylor, J. W., Wu, H., Szpek, K., Bower, K., Crawford, I., Flynn, M. J., Williams, P. I., Dorsey, J., Langridge, J. M.,
935 Cotterell, M. I., Fox, C., Davies, N. W., Haywood, J. M. and Coe, H.: Absorption closure in highly aged biomass
936 burning smoke, *Atmos. Chem. Phys.*, 20(19), 11201–11221, doi:10.5194/acp-20-11201-2020, 2020.

937 Wang, X., Sedlacek, A. J., DeSá, S. S., Martin, S. T., Alexander, M. L., Alexander, M. L., Watson, T. B., Aiken, A. C.,
938 Springston, S. R. and Artaxo, P.: Deriving brown carbon from multiwavelength absorption measurements: Method
939 and application to AERONET and Aethalometer observations, *Atmos. Chem. Phys.*, 16(19), 12733–12752,
940 doi:10.5194/acp-16-12733-2016, 2016.

941 Wang, X., Heald, C. L., Liu, J., Weber, R. J., Campuzano-Jost, P., Jimenez, J. L., Schwarz, J. P. and Perring, A. E.:
942 Exploring the observational constraints on the simulation of brown carbon, *Atmos. Chem. Phys.*, 18(2), 635–653,
943 doi:10.5194/acp-18-635-2018, 2018.

944 Wei, Y., Ma, L., Cao, T., Zhang, Q., Wu, J., Buseck, P. R. and Thompson, J. E.: Light scattering and extinction
945 measurements combined with laser-induced incandescence for the real-time determination of soot mass absorption
946 cross section, *Anal. Chem.*, 85(19), 9181–9188, doi:10.1021/ac401901b, 2013.

947 Westerling, A. L., Hidalgo, H. G., Cayan, D. R. and Swetnam, T. W.: Warming and Earlier Spring Increase Western
948 U. S. Forest Wildfire Activity, *Science*, 313(5789), 940–943, doi:10.1126/science.1128834, 2006.

949 Williams, E. L. and Grosjean, D.: Removal of Atmospheric Oxidants with Annular Denuders, *Environ. Sci. Technol.*,
950 24(6), 811–814, doi:10.1021/es00076a002, 1990.

951 Wonaschütz, A., Hitzenberger, R., Bauer, H., Pournesmaeil, P., Klatzer, B., Caseiro, A. and Puxbaum, H.: Application
952 of the integrating sphere method to separate the contributions of brown and black carbon in atmospheric aerosols,
953 *Environ. Sci. Technol.*, 43(4), 1141–1146, doi:10.1021/es8008503, 2009.

954 Yue, X., Mickley, L. J., Logan, J. A. and Kaplan, J. O.: Ensemble projections of wildfire activity and carbonaceous
955 aerosol concentrations over the western United States in the mid-21st century, *Atmos. Environ.*, 77, 767–780,
956 doi:10.1016/j.atmosenv.2013.06.003, 2013.

957 Zeng, L., Zhang, A., Wang, Y., Wagner, N. L., Katich, J. M., Schwarz, J. P., Schill, G. P., Brock, C., Froyd, K. D.,
958 Murphy, D. M., Williamson, C. J., Kupc, A., Scheuer, E., Dibb, J. and Weber, R. J.: Global Measurements of Brown
959 Carbon and Estimated Direct Radiative Effects, *Geophys. Res. Lett.*, 47(13), doi:10.1029/2020GL088747, 2020.

960 Zeng, L., Sullivan, A. P., Washenfelder, R. A., Dibb, J., Scheuer, E., Campos, T. L., Katich, J. M., Levin, E., Robinson,
961 M. A. and Weber, R. J.: Assessment of online water-soluble brown carbon measuring systems for aircraft sampling,
962 *Atmos. Meas. Tech.*, 14(10), 6357–6378, doi:10.5194/amt-14-6357-2021, 2021.

963 Zeng, L., Dibb, J., Scheuer, E., Katich, J. M., Schwarz, J. P., Bourgeois, I., Peischl, J., Ryerson, T., Warneke, C.,
964 Perring, A. E., Diskin, G. S., Digangi, J. P., Nowak, J. B., Moore, R. H., Wiggins, E. B., Pagonis, D., Guo, H.,
965 Campuzano-jost, P., Jimenez, J. L., Xu, L. and Weber, R. J.: Characteristics and Evolution of Brown Carbon in
966 Western United States Wildfires, *Atmos. Chem. Phys.*, 22, 8009–8036, doi:10.5194/acp-22-8009-2022, 2022.

967 Zhang, L., Segal-Rozenhaimer, M., Che, H., Dang, C., Sedlacek, A. J., Lewis, E. R., Dobracki, A., Wong, J. P. S.,
968 Formenti, P., Howell, S. G. and Nenes, A.: Light absorption by brown carbon over the South-East Atlantic Ocean,
969 *Atmos. Chem. Phys.*, 22(14), 9199–9213, doi:10.5194/acp-22-9199-2022, 2022.

970 Zhang, Y., Forrister, H., Liu, J., Dibb, J., Anderson, B., Schwarz, J. P., Perring, A. E., Jimenez, J. L., Campuzano-Jost,
971 P., Wang, Y., Nenes, A. and Weber, R. J.: Top-of-atmosphere radiative forcing affected by brown carbon in the
972 upper troposphere, *Nat. Geosci.*, 10(7), 486–489, doi:10.1038/ngeo2960, 2017.

973